In the name of God

Communications in Catalysis (Abbreviation: CIC) is an international, open access, online/printed scholarly biannual publication issued by the Department of Chemistry, Azarbaijan Shahid Madani University, Tabriz, Iran. High quality original papers in English dealing with experimental, theoretical and applied research related to catalysis science and technology are welcomed by CIC. This journal provides a forum for publication of original research papers, short communications, and critical reviews in all branches of chemical science and technology, on catalysts and their application in several areas, such as: organic, inorganic, bioorganic, analytical, polymer, etc. Publication process of the manuscripts submitted to CIC is free of charge. All the submitted manuscripts are peer-reviewed by the editorial board and reviewers of the CIC before acceptance for publication. To submit a new manuscript, please start by reading the journal instructions for authors (http: cic.azaruniv.ac.ir).

Prof. D. Nematollahi
(Chemistry Department, Faculty of Science, Buali Sina University, Hamadan, Iran.)
Prof. K. Niknam
(Chemistry Department, Faculty Science, Persian Gulf University, Bushehr, Iran.)
Prof. H. Razmi
(Chemistry Department, Faculty of Science, Azarbaijan Shahid Madani University, Tabriz,Iran.)
Prof.Z.Rezvani
(Chemistry Department, Faculty of Science, Azarbaijan Shahid Madani University, Tabriz,Iran.)
Prof. A. Salimi
(*Department of Chemistry, Faculty of Science, University of Kurdistan, Kurdistan, Iran.)*
Prof. H. Valizadeh
(Chemistry Department, Faculty of Science, Azarbaijan Shahid Madani University, Tabriz,Iran.)

Contents

Communications In Catalysis
Vol. 1, No. 1, 2024, pp.1-10
DOI: 10.22049/CIC.2018.13736

Azarbaijan Shahid Madani University

New strategy to increase comonomer incorporation in LLDPE synthesis using Ziegler-Natta catalysts

Reza Bazvand[a], Naeimeh Bahri-Laleh[a*], Mehdi Nekoomanesh[a], Hossein Abedini[b], Ahad Hanifpour[a]

[a]Polymerization Engineering Department, Iran Polymer and Petrochemical Institute (IPPI), P.O. Box 14965/115, Tehran, Iran.

[b]Process, Modeling and Control Department, Iran Polymer & Petrochemical Institute, P.O. Box 14965/115, Tehran, Iran.

Tel: +982148662479, Fax: 982144787021.

E-mail address: n.bahri@ippi.ac.ir

Received: 2024-02-06, Revised: 2024-02-29, Accepted: 2024-03-10

Abstract

Effect of $FeCl_3$ and $FeCl_3/SiCl_4$-doping on the performance of $MgCl_2$ (ethoxide type)/$TiCl_4$/TEAL catalytic system was evaluated in the linear low density polyethylene (LLDPE) synthesis using 1-hexene as the comonomer. Results revealed that $FeCl_3/SiCl_4$ modified catalytic system has better performance in terms of catalyst activity and comonomer incorporation when compared with unmodified catalyst or the catalytic system in the presence of $FeCl_3$ alone. In fact, the introduction of $FeCl_3$ doper, in its optimum amount of 10 wt. %, together with $SiCl_4$induced better catalytic performance with 212 and 90 % increase in catalyst activity and 1-hexene incorporation, respectively.Copolymers characterization showed increased bulk density together with decreased crystallinity and T_m in the polymers from modified catalysts. Overall results showed that, new catalytic system represented in this work, is a good candidate for large scale LLDPE production with high comonomer amount.

Keywords: LLDPE; modified support; $FeCl_3$; Ziegler-Natta catalyst.

Introduction

Ethylene copolymers are an important class of industrial materials.The properties and processing characteristics of these copolymers are through outsubordinate on the amount and distribution of the comonomers.In light of the vast array of different catalyst combinations for this issue, our understanding of the influences of the modifiers on copolymerization characteristic is still evolving.In the last two decades among the polyethylene family(HDPE, LDPE, and LLDPE), LLDPE had the highest production growth rate[1].LLDPE copolymers are manufactured by the copolymerization of ethylene with higher α-olefin monomer like 1-butene, 4-methyl-1-pentene, and 1-hexene. It is generally known that, α-olefin exists in small amount in the copolymer, leads to short chain branches on the polymer backbone[2]. Most of the LLDPE properties can be affected by these short chain branching.

It is accepted that, a wide range properties of LLDPEs can be resulted by altering the number and distribution of short chain branches. In addition, the length of the short chain branch may also play an important role in governing the mechanical properties of the prepared LLDPE[3, 4].

More than 80 % of LLDPE productions are performed by Ziegler-Natta (ZN) catalysts. In fact, heterogeneous ZN catalyst assisted olefin polymerization, is amongst the most important polymerization reactions [5-7]. Therefore, this catalyst plays a prominent role in LLDPE synthesis due to its low cost, accessibility and high performance [8-11].

Three key ingredients containing i) support ii) $TiCl_4$ embedded on the support surface, and iii) an Al-alkyl cocatalyst compose industrial ZN system. $MgCl_2$and $Mg(OEt)_2$ are preferred supports in this case since Mg and Ti have similar atomic radii. Although, $Mg(OEt)_2$ precursor is mainly converted to related $MgCl_2$ during titanation step, ZN catalysts prepared from $Mg(OEt)_2$ precursor received a lot of attention among studied supports due to higher overall catalytic activity [12].As a result, many industrial HDPE and LLDPE plants employ $MgCl_2$ (ethoxide type)/$TiCl_4$ as the active catalyst precursor.

One of the disadvantages in heterogeneous ZNcatalytic system is its low efficiency toward higher α-olefins which lead to low comonomer incorporation in ethylene/α-olefin copolymers. Although many reports describe the preparation of highly active ZN catalyst in ethylene/α-olefin copolymerization [8], however a catalyst with optimal activity and selectivity toward higher α-olefins has not been achieved yet and many concepts are still under discussion.

It was accepted that metal halide derivatives, which can be added to $Mg(OEt)_2$or $MgCl_2$supports, have the ability to change surface properties of them, resulting in the modification of active center distribution of catalysts[13]. Their addition to catalyst systems consequently lead to the improvement in catalytic performance (i.e. catalyst activity and comonomer incorporation) and polymer properties [14-17].

In this study the performance of the $MgCl_2$ (ethoxide type)/$TiCl_4$catalyst in the

presence of $FeCl_3$ dopant and $SiCl_4$ modifier is concerned in slurry phase LLDPE synthesis. Activity results of the represented modifier furnishes this catalytic system as a good candidate for large scale LLDPE production with increased polymer yield and high comonomer content.

Experimental

Materials

Mg $(OEt)_2$, $SiCl_4$, $FeCl_3$, THF, and $TiCl_4$ (99 %) were purchased from Merck (Darmstadt, Germany). Ethylene gas in polymerization grade was obtained from Arak Petrochemical Co. (Arak, Iran) and was further purified and dried by passing through purification unit containing molecular sieve filled columns. Toluene and n-hexane were kindly donated by Bandar Imam Petrochemical Co. (Mahshahr, Iran). Triethylaluminum (TEA) cocatalyst and 1-hexene comonomer were purchased from Sigma-Aldrich Chemical Co. (St. Loius, MO, USA). Nitrogen gas with 99.99 % purity was provided from Roham Co. (Tehran, Iran).

Catalyst synthesis

Preparation of the catalysts was carried out
according to our previous work[18].A typical procedure is as follows:

First, doped supports were prepared by blending appropriate amounts of Mg $(OEt)_2$ and $FeCl_3$ in THF by vigorous stirring of the mixture at 63 °C and at N_2 atmosphere. After 8 h, the prepared support was separated from the solvent and dried under inert atmosphere at60 °C within 3 hour.

To synthesize the catalysts, 2.0 g of the support was added in to a 250 mL two-necked glass reactor containing 50 mL of toluene under N_2 atmosphere at 50 °C. After 30 min stirring, the temperature was gradually raised to 80 °C. Then, 8 mL $TiCl_4$ was added drop wise to the solution. After 4 h, the supernatant was removed, and thesolid residue was washed twice with 100 mL of toluene and 4 times with 100 mL of dry hexane to remove unreacted $TiCl_4$. The final catalyst was subsequently dried under a flow of hot N_2during 2 h.The characteristic and abbreviation of the synthesized catalysts is summarized in Table1.

Table 1. Labels, abbreviations, and composition of the synthesized catalysts.

Catalyst name	$SiCl_4$*	$Mg(OEt)_2/FeCl_3$ w/w ratio	Ti (wt%)
F_0	NO	100/0	7.78
F_5	NO	5/95	6.40
F_{10}	NO	10/90	4.69
F_{15}	NO	15/85	3.81
F_5-Si	YES	5/95	5.98
F_{10}-Si	YES	10/90	4.41

F_{15}-Si	YES	15/85	3.12

*$SiCl_4$ was added during catalyst synthesis before the addition of $TiCl_4$

Copolymerization procedure

Ethylene/1-hexene copolymerization was carried out in a 1-L Buchi stainless steel reactor (Buchibmd 300, Switzerland) equipped with an anchor type mechanical stirrer. The reactor was charged with 500 mL hexane, 0.15 mol of 1-hexeneand appropriate amount of TEAL to reach Al/Ti=180. After 5 min stirring at 83 °C,10 mg of the synthesized catalyst was added to the reactor and then ethylene gas was fed to induce a reactor pressure of 5 bars.After 1 h stirring, the reaction was stopped, and the product was evacuated and dried under vacuum in80 °C.

Measurements

Comonomer content was measured according to ASTM D 2238 –68 standard test method. This method is based on the side chain methyl groups absorbance of polymer at 1376 cm^{-1}[19]. A Nicolet IS5 FT-IR (USA) instrument was used for the determination of methyl group absorbance in polyethylene chain.Morphology of the synthesized catalysts was observed with a VEGA SEM instrument (TESCAN, Czech Republic).The DSC tests were performed on a DSC Mettler Toledo (Switzerland), under nitrogen atmosphere at a heating rate of 10 °C/min. Degree of crystallinity (X_c) and melting temperature (T_m) were obtained from the second heating scan. X_c was calculated according to the following equation:

$$X_C = \frac{\Delta H_m}{\Delta H_m^+}$$

Where, ΔH_m^+ is the specific melting enthalpy of 100 % crystalline PE (288 J/g) [18]and $\Delta H_m$is specific enthalpy of melting of the sample.

Results and discussion

$FeCl_3$doped $Mg(OEt)_2/TiCl_4$ ZN catalysts, which was just reported in our previous papers[13, 18], had a simple preparation procedure and showed high activity in ethylene homopolymerization. Here we discuss the effect of $FeCl_3$ doping on catalyst activity and comonomer incorporation in ethylene/1-hexene copolymerization. In this regard, Mg $(OEt)_2/FeCl_3/TiCl_4$ catalysts containing 0, 5, 10 and 15 w/w % of $FeCl_3$ in the support structure were synthesized in the presence as well as absence of $SiCl_4$. Catalysts compositions and the abbreviations has been shown in Table 1.

According to the activity results ofFigure1, by increasing $FeCl_3$ amount up to 10 %, activity increased from 185 kg Polym/g Ti·hin undoped catalyst (F_0) to 241 and 368 kg Polym/g Ti·hin F_5 and F_{10}, respectively. Thereafter, by further increase in the $FeCl_3$ amount, a drastic drop in the catalyst activity (-22 %) was observed for F_{15} catalyst. In Fe-Si doping cases, activity increased from 185 kg Polym/g Ti·hin F_0catalyst to 277 kg Polym/g Ti·h in F_5-Si and then reached its maximum amount of 577 kg Polym/g Ti·hin F_{10}-Si, while by further increase in Fe amount to 15 %, catalyst activity dropped as an order of 60 %.

The mechanism of halogen containing modifiers promotion effect in ZN catalysts is still evolving. However, as it had already been shown, $SiCl_4$ on the catalyst structure can act as a promoter and cause

an increase in the catalyst activity [9, 13, 20].

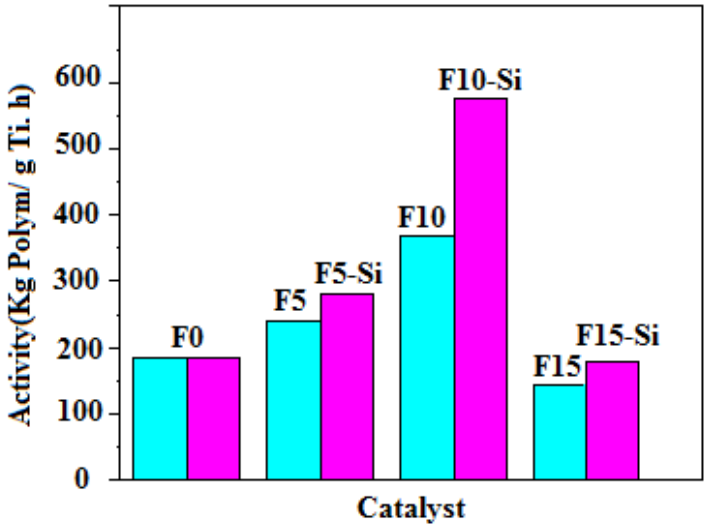

Figure1. Calculated activities for ethylene/1-hexene copolymerization using synthesized catalysts

Comonomer content characterization of the samples has been carried out using FT-IR spectra (Figure 2). In these spectra, the observed bands at 2957, 2920 and 2851 cm^{-1}related to the C-H stretching vibrations of CH_3, CH_2 and CH groups, 1630 and 720 cm^{-1} to the C=C stretching and bending,1468 and 1376 $cm^{-1}$to the deformation of CH_2 and CH_3 groups, respectively[21]. Comonomer content analysis of the synthesized copolymers was summarized in Figure3.Obtained results emphasized that, modification of the catalyst with $FeCl_3$ and combined $FeCl_3/SiCl_4$ lead to dramatic increase (from 2.8 % in F_0 to 4.2 and 5.4 % in F_{10} and F_{10}-Si catalysts, respectively) in the comonomer incorporation.In crescent of comonomer content with modification of the catalyst with $FeCl_3$ and combined $FeCl_3/SiCl_4$ may be due to several reasons as the following:

a) $FeCl_3$ is a stronger Lewis acid in comparison to $MgCl_2$, so the presence of $FeCl_3$ in the catalyst can decrease the density of electrons in active centers and make suitable active centers toward 1-hexeneinsertion[13].

b) the presence of $FeCl_3$ in the catalyst leads to a change in type and distribution of active centers on its surface and in consequence, it constitutes active centers with high capability for copolymerization[22].

c) the presence of $FeCl_3$ in the catalyst leads to diminishing of mechanical properties of the catalyst by the appearance of some cracks in the catalyst surface (see Figure 4), so the disintegration of the catalyst particles occurs easier. This lead to higher catalyst activity in doped supports.

Morphologies of catalysts obtained from scanning electron microscopy (SEM) were shown in Figure 4. As it is obvious from that Figure, all of catalysts showed almost spherical morphology. Detailed examination of the pictures revealed that with the addition of $FeCl_3$, narrow cracks

appeared at the catalysts surface (Figure 4-b and 4-c). These cracks made catalyst fracture easier and lead to higher catalytic activity.

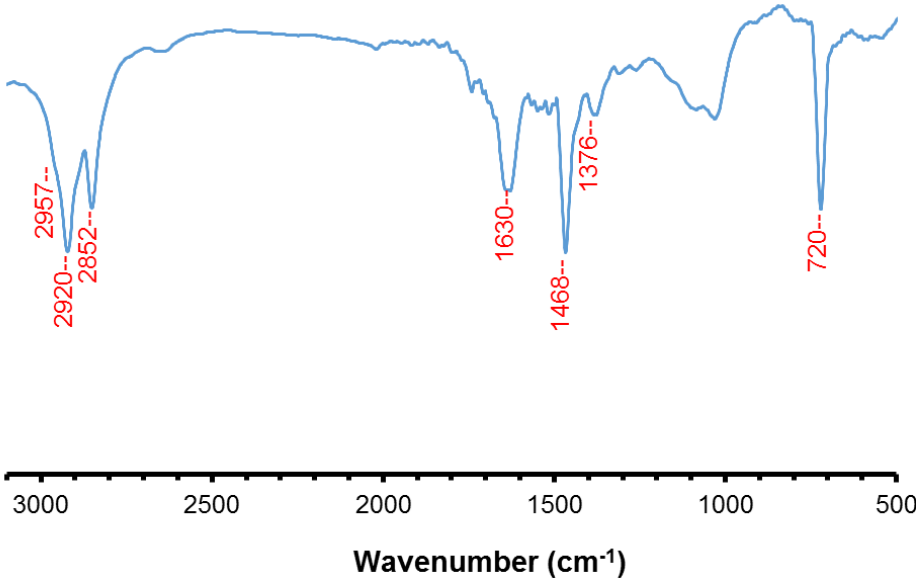

Figure 2. FT-IR spectrum of the synthesized copolymer with F_5 catalysts as an example.

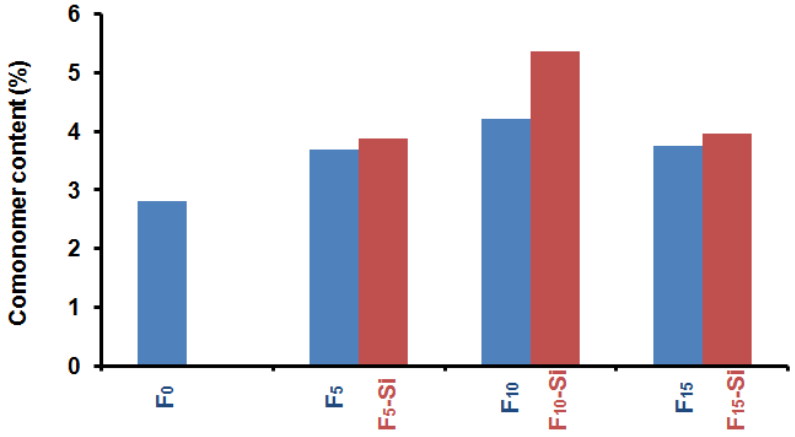

Figure 3. Comonomer incorporation abilities of the synthesized catalysts in ethylene/1-hexene copolymerization

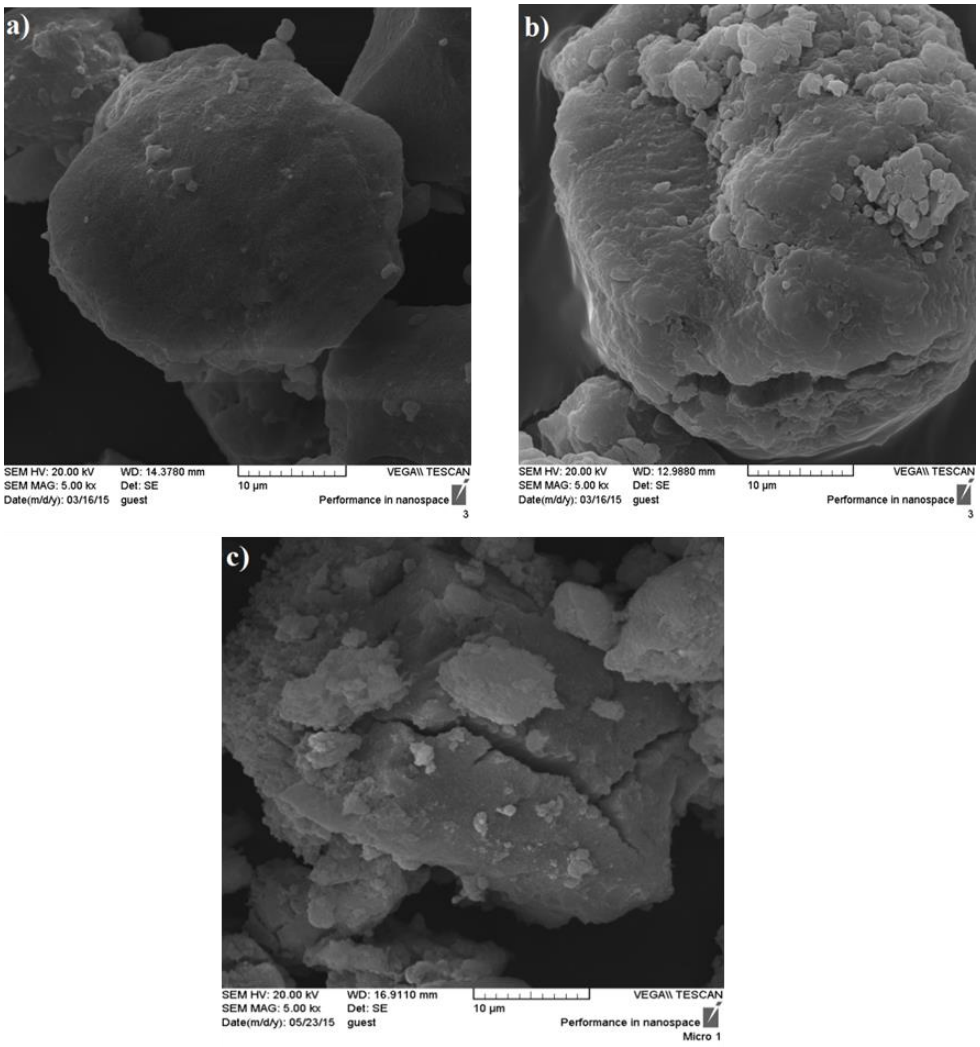

Figure 4. SEM images of synthesized catalysts: a) F_0, b) F_{10}; and c) F_{15}

In order to investigate crystallinity and thermal properties of the produced copolymers with different catalysts, differential scanning calorimetry(DSC) was conducted at a heating rate of 10 °C/min [23-25].Obtained curves were shown in Figure5 and the results were collected in Table 2. According to the data of Table 2, produced copolymers by catalysts containing 5 and 10 % $FeCl_3$ and combined $FeCl_3/SiCl_4$ had less melting temperature and crystallinity percentage in comparison to the unmodified catalyst (F_0), so that, the melting temperature and crystallinity percentage of the produced copolymers decreased from 131.6 °C and 53 % in unmodified catalyst to a range of 128.7-130.4 °C and 44-47 % in the modified catalysts, respectively (Figure5). This decrease in X_c and $T_m$is an evidence of increased comonomer amount in the backbone of the copolymers [26-29].

On the other hand, T_m and X_c of the produced polymers via F15 and F15-Si catalysts increased again. The advent of such effect is unclear to us and needs further consideration.

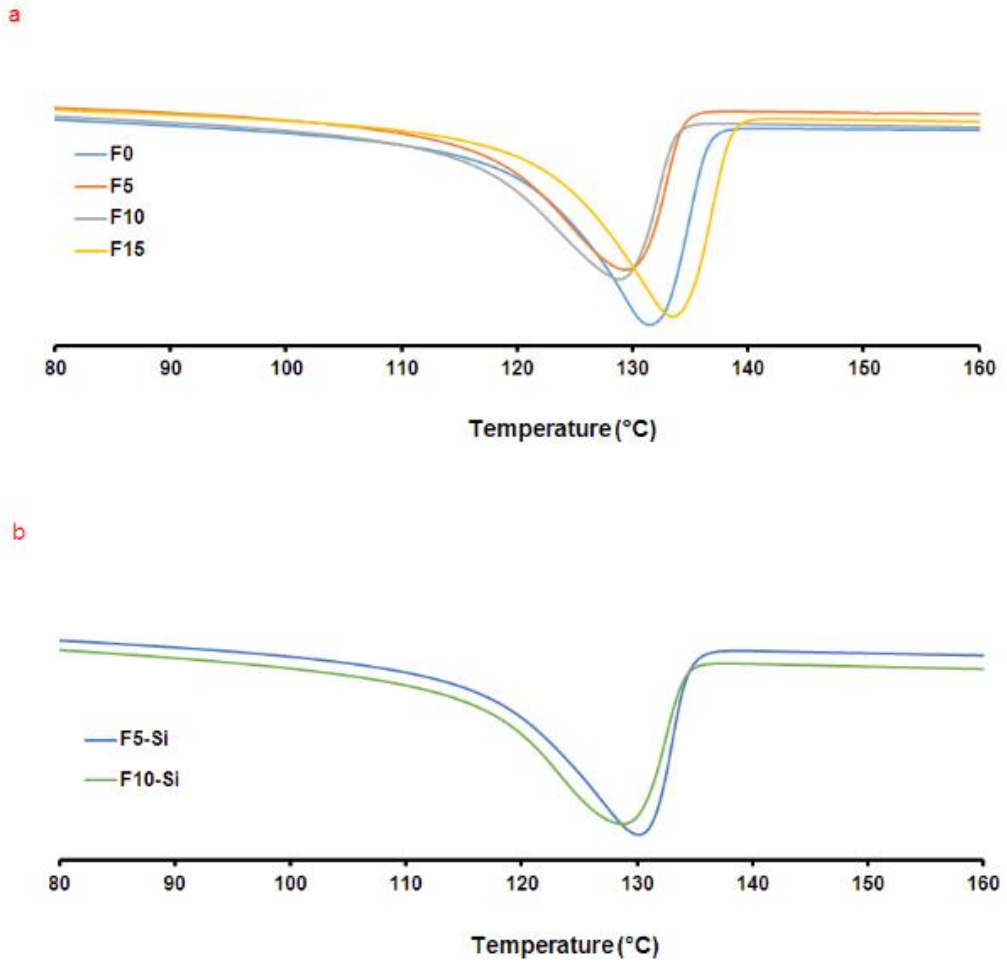

Figure5. DSC curves of prepared samples with a) $FeCl_3$-doped, and b) $FeCl_3/SiCl_4$-doped catalysts

Table 2. Results of DSC, and bulk density characterization of ethylene\1-hexene copolymers produced via different catalyst systems.

Catalyst code	F_0	F_5	F_{10}	F_{15}	F_5-Si	F_{10}-Si	F_{15}-Si
Crystallinity (%)	53	47	46	53	45	44	53
T_m (°C)	131.6	130.4	129.0	133.4	130.4	128.7	132.0
Bulk density (gr/ml)	0.22	0.34	0.37	0.30	0.34	0.37	0.31

The bulk density of produced copolymers increased drastically from 0.22 g/mL to a range of 0.30-0.37 g/ml in the produced copolymers with modified catalysts (see Table2). The increase in the bulk density of produced copolymers with doped

catalysts can be attributed to the presence of $FeCl_3$ in the catalyst which caused catalyst breakage to occur easier in the polymerization pool, subsequently a smaller copolymer particle size was produced which raised bulk density.

Conclusions

Linear low density polyethylene (LLDPE) as synthesized by a series of $FeCl_3$ and $FeCl_3/SiCl_4$modified $MgCl_2$ (ethoxide type)/$TiCl_4$ catalytic system using 1-hexene as comonomer.Obtained copolymers were characterized in terms of their comonomer content, catalyst activity, bulk density, crystallinity, and melting point.The catalyst activity profile showed that in the presence of suitable amount of $FeCl_3$,catalyst activity increases, whereas decrease of the catalyst activity was observed in higher $FeCl_3$ content. DSC analysis demonstrated that the melting temperature and crystallinity percentage of the produced copolymers were decreased compared to obtained copolymer from pristine catalyst.With doping of $FeCl_3$ /$SiCl_4$ to the catalytic system, comonomer content and bulk density of the copolymers increased as well. Our results suggested new/modified catalytic system which has better performance in terms of catalyst activity and comonomer incorporation than old/conventional ZN catalyst based on $TiCl_4/MgCl_2$in LLDPE synthesis.

References

[1] Bahri-Laleh, N.; Nekoomanesh, M.; S., S.; Pajouhan, A. Polyolefins. J. 2016, 3, 11.

[2] Gupta, P.; Wilkes, G. L.; Sukhadia, A.M.; Krishnaswamy, R. K.; Lamborn, M. J.; Wharry, S. M.; Tso, C. C.; DesLauriers, P. J.; Mansfield, T.; Beyer, F. L. Polymer. 2005, 46 (20), 8819..

[3] Tarasova, E.; Poltimäe, T.; Krumme, A.; Lehtinen, A.; Viikna, A. Macromol.Symp. 2009, 282 (1), 175.

[4] Hong, H.; Zhang, Z.; Chung, T. C. M.; Lee, R. W. J. Polym. Sci A Polym. Chem. 2007, 45 (4), 639.

[5] Bahri-Laleh, N.; Poater, A.; Cavallo, L.; Mirmohammadi, S. A., Dalton. Trans. 2014, 43 (40), 15143.

[6] Bahri-Laleh, N. Appl. Surf. Sci. 2016, 379, 395.

[7] Correa, A.; Bahri-Laleh, N.; Cavallo, L. Macromol. Chem. Phys. 2013, 214 (17), 1980.

[8] Hadian, N.; Hakim, S.;Nekoomanesh - Haghighi, M.; bahri-Laleh, N. Polyolefins. J. 2014, 1 (1), 33.

[9] Phiwkliang, W.; Jongsomjit, B.; Praserthdam, P. Chin. J. Polym. Sci.2014**,**32 (1), 84.

[10]Rahbar, A.; Nekoomanesh-Haghighi, M.; Bahri-Laleh, N.; Abedini, H.Catal. Lett.2015, 1.

[11]Bahri-Laleh, N.; Arabi, H.; Mehdipor-Ataei, Sh.; Nekoomanesh-Haghighi, M.; Zohuri, GH.; Seifali, M.; Akbari, Z. J. Appl. Polym. Sci.2012**,**123, 2526.

[12]Takahashi, S.; Wada, T.; Chammingkwan, P.; Taniike, T.; Terano, M. Macromol. React. Eng.2017, In press.

[13]Nouri-Ahangarani, F.; Bahri-Laleh, N.; Nekomanesh Haghighi, M.; Karbalaei, M. Des. Monomers. Polym.2016**,**19 (5), 394.

[14]Chen, Y.-p.; Fan, Z.-q., Eur. Polym. J**.**2006**,**42 (10), 2441.

[15]Phiwkliang, W.; Jongsomjit, B.; Praserthdam, P.; Taniike, T.; Terano, M.,8thinternational colloquium on

heterogeneous Ziegler-Natta catalyst, Kanazava, Japan, 2012.
[16]Britto, M. L.; Galland, G. B.; dos Santos, J. H. Z.; Forte, M. C. Polymer**.** 2001**,**42, 6355.
[17]Kaivalchatchawal, P.; Samingprai, S.; Shiono, T.; Praserthdam, P.; Jongsomjit, B. Eur. Polym. J.2012**,**48 (7), 1304-1312.
[18] Bazvand, R.; Bahri-Laleh, N.; Nekoomanesh-Haghighi, M.; Abedini, H. Des. Monomers. Polym.2015**,**18 (7), 599
[19] Standard Test Methods for Absorbance of Polyethylene Due to Methyl Groups at 1378 cm^{-1}. ASTM International: West Conshohocken, PA, 2012.
[20]Phiwkliang, W.; Jongsomjit, B.; Praserthdam, P. J. App. Polym. Sci.2013***,130*** (3), 1588.
[21]Kuila, T.; Bose, S.; Mishra, A. K.; Khanra, P.; Kim, N. H.; Lee, J. H. Polym. Test.2012**,**31 (1), 31.
[22]Luo, H. K.; Tang, R. G.; Yang, H.; Zhao, Q. F.; An, J. Y., Appl. Catal. A2000**,**203, 269.
[23]Mehdipour-Ataei, S.; Amirshaghaghi, A.; Bahri, N.Eur. Polym. J.2006**,**42 (10), 2646.
[24]Mirmohammadi, S. A.; Imani, M.; Uyama, H.; Atai, M.; Teimouri, M. B.; Bahri-Lale, N., Polym. Int.2014**,**63 (3), 479.
[25]Mehdipour-Ataei, S.; Bahri-Laleh, N., Polym. Adv.Technol. 2008**,**19 (4), 291.
[26]Czaja, K.; Białek, M.; Utrata, A. J. Polym. Sci. A: Polym. Chem.2004**,**42 (10), 2512.
[27]Echevskaya, L. G.; Matsko, M. A.; Mikenas, T. B.; Nikitin, V. E.; Zakharov, V. A. J. Appl. Polym. Sci.2006**,**102 (6), 5436.
[28]Matsko, M. A.; Echevskaya, L. G.; Mikenas, T. B.; Nikolaeva, M. I.; Vanina, M. P.; Zakharov, V. A.Cataly. Ind.2011**,**3 (2), 109.
[29]Fu, T.; Cheng, R.; He, X.; Liu, Z.; Tian, Z.; Liu, B. Polyolefins. J.2016**,**3 (2), 103.

Communications In Catalysis
Vol. 1, No. 1, 2024, pp.11-19
DOI: 10.22049/CIC.2018.13722

Azarbaijan Shahid Madani University

Synthesis of neopenthylglycolesters using homogeneous and heterogeneous catalysts as synthetic lubricant base oils

HADI JABBARI

Department Of Chemistry, Payame Noor University, PO BOX 19395-4697 Tehran, Iran.

Email:Hadijabbari@yahoo.com,tel:(+98)4433653791,Fax: (+98)4433653791.

Received: 2024-02-25, Revised: 2024-03-11, Accepted: 2024-03-20

Abstract

The preparation of Neopenthylglycol (NPG) esters via esterification reaction of Neopenthylglycol by carboxylic acid in the presence of solid acidic catalysts has been investigated. The used catalysts were natural zeolite, acidic ion exchange resin catalyst (polyestyrendivinylbenzensulfated), synthetic zeolites (ZEOKAR-2, ASHNCH-3), heteropolyacid $H_4Si\ (W_3O_{10})_4$, and sulfated metal oxid ZrO_2.The reactions were carried out under solvent-less conditions. It was observed that sulfated ZrO_2 has higher reactivity and efficiency among the investigated catalysts. For this purpose esterification of ethylenglycol,trimethylolpropan Using sulfated ZrO_2 by carboxylic acids has been investigated.

Keywords: Esterification, Solid catalyst, Zeolite, Sulfated zirconia, NPG.

Introduction

Plasticizers are important class of low molecular weight nonvolatilecompounds that are widely used in the polymerindustries [1]. Some commercially available plasticizers such asdibutyl phthalate (DBP), di-iso-butyl phthalate (DIBP), di-isopentylphthalate (DIPP), di-iso-heptyl phthalate (DIHP),and dioctyl phthalate (DOP) are normally prepared via theesterification reaction of phthalic anhydride by the correspondingalcohols in the presence of acidic catalysts [2-4]. Amongplasticizers, dioctyl phthalate (DOP), DOA (dioctyladipate),and dioctyl terephthalate (DOTP) have been found wideapplications due their biocompatibility [5-7]. And co-workers.Heteropolyacids are widely used in variety of acid catalyzed reactions such as esterification [8, 9] etherification hydration of olefin deesterification [10] dehydration of alcohol [11] and polymerization of THF [12] in homogenous and heterogeneous systems. Their application the production of DOP was also reported. The catalytic activity of some $AlPO_4$ molecular such as AlPO4-12, etc. in the esterification reaction of propinic acid with n-butanol has been investigated [13]. Preparation of DOP (dioctylphetalat) using silicoaluminophosphate molecular sieve HSAPO-1 has also reported by Zhao [14].

Among various sulfated metal oxides, sulfated zirconia has attracted much attention and has been extensively investigated during the last two decades [15, 16] The major concern of this research still focuses on the acidity, in terms of types Sulfated zirconia catalyst, promoted with iron aluminum and manganese, has shown much higher activity and could isomerize n-butane at 35°C under normal pressure in a continuous-flow recirculation tank reactor. Zeolites are widely used within the petrochemical industry in acid catalyzed processes, and there are several reviews concerning recent developments in their use in the synthesis of fine and specialty chemicals [17-20]. For this purpose esterification of polyol alcohols by carboxylic acids has been investigated. It was observed that sulfated zirconia is an effective catalyst for this purpose. Zirconia is an effective catalyst for this purpose.

Experimental

General

Neopenthylglycol,Ethylenglycol(99% purity),pentanoicacid (99% purity), caprice acid (98% purity), heptanoicacid (99% purity), were obtained from Merck Chemical Co. Heteropolyacid acid $H_4Si(W_3O_{10})_4$, CAS No. 12027-38-2, inthe form of white to light yellow crystalline solid),polyestyrendivinylbenzensulfated and p-Toluenesulfonic acid were purchased from Merck Chemical. And used without further purification. Natural Zeolite (Clinoptilolite was obtained from “Iran Zeolite Co.” (Tehran, Iran). It was activated before use by refluxing in 60% H_2SO_4 solution for 2 h, washing with hotwater until neutralization (filtrated was checked by pH paper), and then drying at 450–500°C for 3 h. ZEOKAR-2 and ASHNCH-3 are synthetic zeolites and

purchased from YUKOS Co. (Russian). They have been activated by heating at 550–600°C for 3 h.

Table 1: Characteristics of the natural and synthetic Zeolites [21]

Physicochemical properties	ASHNCH-3	ZEOKAR-2	Natural Zeolit
%2 SiO	83.0-85.0	83.0-89	62.0-69
$\%Al_2O_3$	9.0-11.0	9.0-15.0	10.0-12.0
$\%_2O_3Fe$	-	0.2>	0.8-1.0
%CaO	-	-	0.3-1.0
$\%Na_2O$	0.3	0.7>	5.0-6.5
$\%_2OK$	-	-	2.0-4.0
sRare earthoxid	2.3	-	-
Density	0.69-0.7	0.62-0.7	0.85-1.0
$(^3)$dm/Kg			
size particle (mm)	2.5-5.0	2.5-5.0	1.46-2.46
Color	white	Gray	reenLightg

Typical procedure for preparation of diol esters

Fatty acid and alcohol was transferred into a reaction flask. The reaction flask was equipped with a modified Dean – Stark distillation set-up, magnetic stirrer, condenser, dropping funnel and heating plate. 100cc of toluene is added to the reaction mixture. Heating continued for not more than 5 hours. Water formed as by-product of the esterification reaction was removed continuously by means of distillation with the aid of toluene while toluene was recycled continuously back to the reaction mixture. After the reaction was completed, the crude product was cooled to ambient temperature. Then, heterogeneous acid catalyst was removed by simple filtration and excess solvent was removed from the crude product by means of rotary evaporation. The product was dried with anhydrous sodium sulphate and the hydratedsodiumsulphate was removed from the dried product. The dried product was further purified by using a column packed with silica gel. Trace solvent was further removed by a vacuum pump and finally unreacted fatty acid was removed by vacuum distillation. Unreacted fatty acid would remain as residue while Polyol esters would be collected as distillates.

Instrumentation

^{1}H-NMR ($CDCl_3$) and FT-IR (neat) spectra were recorded on a Bruker-spectrospin-Avance 400-ultra shield spectrumeter and a Shimadzu 200-91527 spectrophotometer, respectively.

Spectra data neopenthylglycoldicaproat ester

^{1}H-NMR:δ(ppm) 0.89 (t ,J=7.5Hz, 6H ,2 CH_3) ,0.96 (s ,6H $2CH_3$), 1.30 (m,8 H , $4CH_2$), 1.62 (quin , J= 7.2Hz ,4H , $2CH_2$), 2.30 (t, J=7.5Hz, 4H ,$2CH_2CO$), 3.87(s, 4H, $2CH_2O$), 3.87 (s , 4H , $2CH_2O$).
^{13}C- NMR δ (ppm)13.77 , 21.67, 22.20, 24.58, 31.22 , 34.15 , 34.56 , 68.90 , 173.58.FT-IR: $\bar{\upsilon}$ (cm^{-1}) 2958 , 2869 , 1739 , 1466 , 1378 , 1244 , 1168 , 1104 , 1006 .

Spectra data neopenthylglycoldipentanoat ester

^{1}H-NMR:δ (ppm) 0.91 (t ,J=7.5Hz, 6H ,2 CH_3) ,1.33 (quin,J=7.2Hz, 4H, $2CH_2$), 1.60 (quin, J=7.5 Hz ,4H, $2CH_2$), 2.32 (t, J= 7.5, 4H , $2CH_2CO$), 4.26 (s, 4H, $2CH_2O$) FT-IR: $\bar{\upsilon}$ (cm^{-1}) 2955, 2867, 1741, 1459, 1378, 1241, 1167, 1105 ,1061 , 965

Spectra data ethylenglycoldicaproat ester

^{1}H-NMR : δ(ppm) 0.86 (t ,J=6.3Hz, 6H ,2 CH_3) ,1.29 (bs , 8H, $4CH_2$), 1.61 (quin, J=6.3Hz ,4H, $2CH_2$), 2.31 (t, J= 7.5, 4H , $2CH_2CO$), 4.26 (s, 4H ,$2CH_2O$).^{13}C NMRδ (ppm)13.82 , 22.24 , 24.52 , 31.21 , 34.04 , 61.93 , 173.50.FT-IR: $\bar{\upsilon}$ (cm^{-1}) 2956 , 2868 , 1742 , 1450 ,1379 , 1347 ,1277 ,1242 , 1167 , 1105 ,1060 ,965.

Spectra data ethylenglycoldiheptanoat ester

^{1}H-NMR: δ(ppm) 0.86 (t ,J=7.5Hz, 6H ,2 CH_3) ,1.27 (m ,12H , 7.2Hz , $6CH_2$), 1.58 (quin, J=7.2 Hz ,4H, $2CH_2CO$), 2.30 (t, J= 7.5Hz ,4H , $2CH_2$), 4.25 (s, 4H ,$2CH_2O$) ^{13}C- NMR :δ (ppm) 13.93 , 22.42 , 24.81 , 28.72 , 31.39 , 34.10 , 61.95 , 173.54.FT-IR: $\bar{\upsilon}$ (cm^{-1}) 2955 , 2867 , 1741 , 1459 ,1378 , 1241, 1167, 1105 , 1061 , 965 cm^{-1}

Spectra data trimethylolpropantricaproat ester

^{1}H-NMR ($CDCl_3$, 400MHz) δ (ppm) 3.98 (s, 6H) ,2.27 (t, 6H, J= 7.6Hz), 1.54(quin, 6H, J=7.4Hz), 1.44(q, 2H, J= 7.6), 1.26 (m, 12H), 0.86(t, 3H, J=7.2), 0.85(t, 9H, J =7.6 Hz).^{13}C NMR ($CDCl_3$, 400MHz) δ(ppm) 172.39, 62.59 , 39.5 , 33.09 , 30.18 , 23.52 , 21.93 , 21.19 , 12.78. FT-IR: $\bar{\upsilon}$ (KBr) 2970, 2930, 2865, 1740,1465,1250,1100 cm^{-1}.

Result and discussion

Esterification of NPG by acid takes place in two stages. The first stage is so rapid that it can be carried out in the absence ofcatalyst. However, esterification of the second carboxylic group is very slow and needs to be facilitated by acid catalyst and the resulting water must be removed from the reaction mixture. (Scheme 1).

The characteristics features of the used natural and synthetic zeolites are given in Table 1. The investigated catalysts were easily separated from the product by simple decantation. The reactions conversions were determined by measuring the acid number of the obtained crude reaction mixture. The obtained products were characterized by FT-IR, ^{13C}-NMR, and ^{1}H-NMR spectroscopies. Reactions condition and conversions for the investigated catalysts are given in Table2. Using of p-toluenesulfonic acid, which is ahomogeneous catalyst was carried out for comparison.

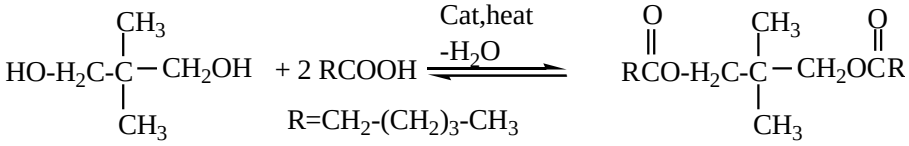

Scheme 1: Preparation of Neopenthylglycol ester

Table2: Reaction conditions and conversions of NPG synthesis by various catalysts[22].

Entry	Catalyst	Catalyst (g/mol C6)[a]	NPG/C6 (molarratio)[b]	Toluene (ml/mol NPG)	Reaction Temperature(°C)	Reaction time (min)	Conversion[c] (%)
1	PTSA[d]	4.5	3.4	150	100	240	98.7
2	ZEOKAR-2	40.5	3.2	-	110-190	240	58.7
3	ASHNCH-3	40.5	3.2	-	110-190	240	63.5
4	Natural Zeolite	40.5	3.6	-	110-190	240	87.7
5	$H_4Si(W_3O_{10})_4$	20.5	3.6	-	100-180	100	89.6
6	Sulfated ZrO_2	30.3	3.6	-	100-200	240	98.7
7	Sulfated ZrO_2	40.5	3.6	-	110-200	240	99.1
8	Sulfated ZrO_2	48.0	3.6	-	110-200	240	99.1
9	Sulfated ZrO_2	40.5	3.6	-	110-200	85	97.5
10	Sulfated ZrO_2	40.5	3.6	-	110-200	105	98.6

aCaproic acid
b.Neopenthylglycol.
c Calculated based on acid number.
d*p*-Toluene sulfonic acid

The important aspect of the present work is caring out the reaction under solvent free condition. This is very important points from economic and environmental views. Sulfatedzirconia showed the maximum reactivity among other catalysts within 4 h. The observed reactivity order of the investigated catalysts is as follow.

Sulfated ZrO_2~p-toluene sulfonic acid >natural zeolite> ASHNCH-3 > ZEOKAR-2> acidic ion exchange resin catalyst (polyestyrendivinylbenzensulfated)

Although the reactivity of the remaining catalysts is lower than homogeneous p-toluene sulfonic acid, but it must be noted they have easy work-up and they use without any solvent. Except in entry 5, heteropolyacidH4Si $(W_3O_{10})_4$ the neutralization and washing steps are omitted for heterogeneous catalysts. Removing of catalyst residue from the obtained product is a part of work-upwhen p-toluenesulfonic acid (entry 1) and heteropolyacid H_4Si $(W_3O_{10})_{4is\ pre}$is used. The data given in Table 2 also show that increasing the amount of sulfated ZrO_2 up to 48.0 g/mol of Caproic acid has not significant effect on the reaction conversion.Within 85min using this catalyst (entry 9), only small change takes place in the reaction conversions refer to other time (entries 10, 6).

Neopenthylglycoldicaproateester, This ester was prepared according to the general

procedure by using Neopenthylglycol (1 mole) and caproeic acid (2moles).

Its ^{1}H-NMR spectrum in chloroformshowed a triplet at δ = 0.89 ppm with J=7.5Hz for two methyl groups, a singlet at δ=0.96 ppm for two methylene groups, a multiplet at δ=1.30 ppm for four methylene groupsnext to carbonyl group,

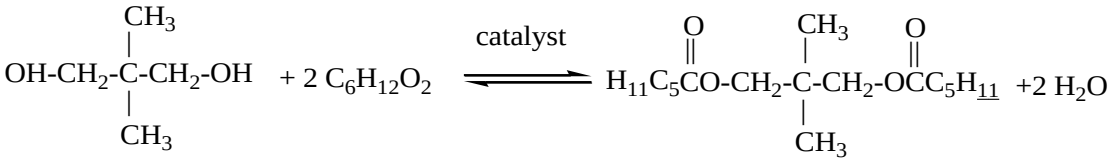

Scheme 2: Preparation of Neopenthylglycoldicaproate ester

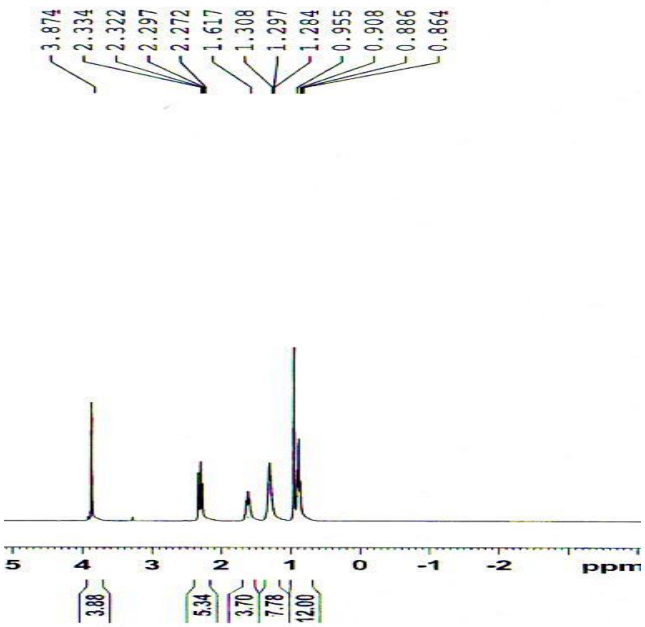

Scheme 3. ^{1}H-NMR Spectrum of Neopenthylglycoldicaproate ester

a quintet at δ=1.62 ppm with J=7.2 Hz for two methylene groups, and triplet at δ=2.30 ppm for next two methylene group , and singlet at δ=3.85-3.87 for four methylene groups next to oygene.

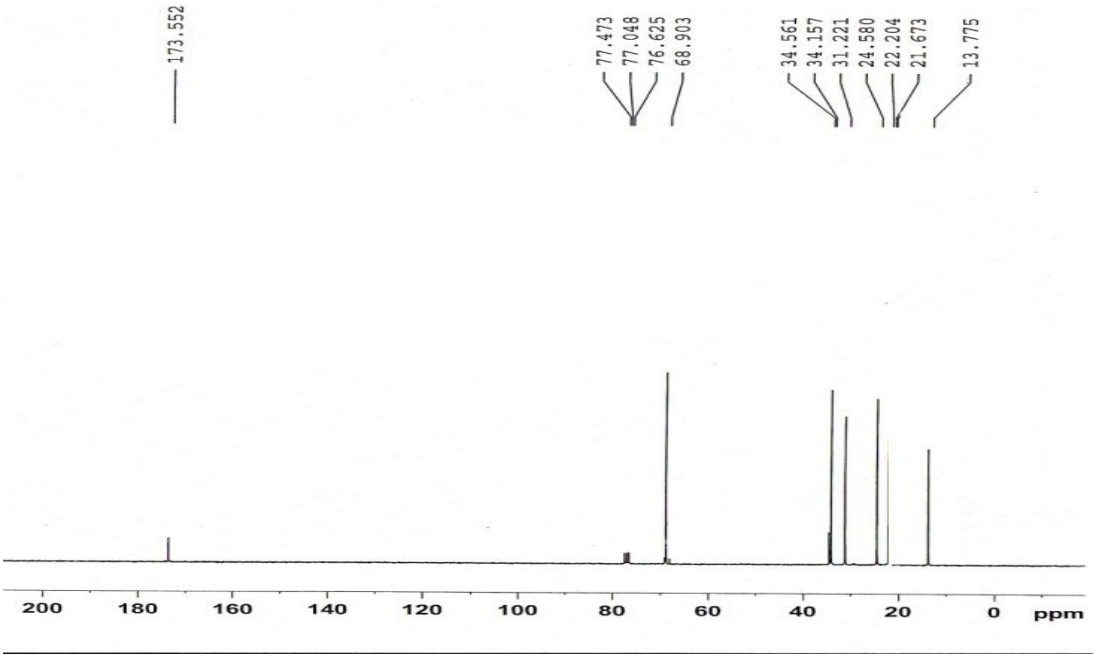

Scheme 4 .[13]C-NMR Spectrum of Neopenthylglycoldicaproate ester

Its [13]C-NMR showed nine peaks for nine different carbons of which the peak at δ=173.58 ppm was due to carbonyl groups.

The peak at δ =68.97 ppm was due to carbon of methylene next to oxygene and other peaks are due to aliphatic alkyl chain.

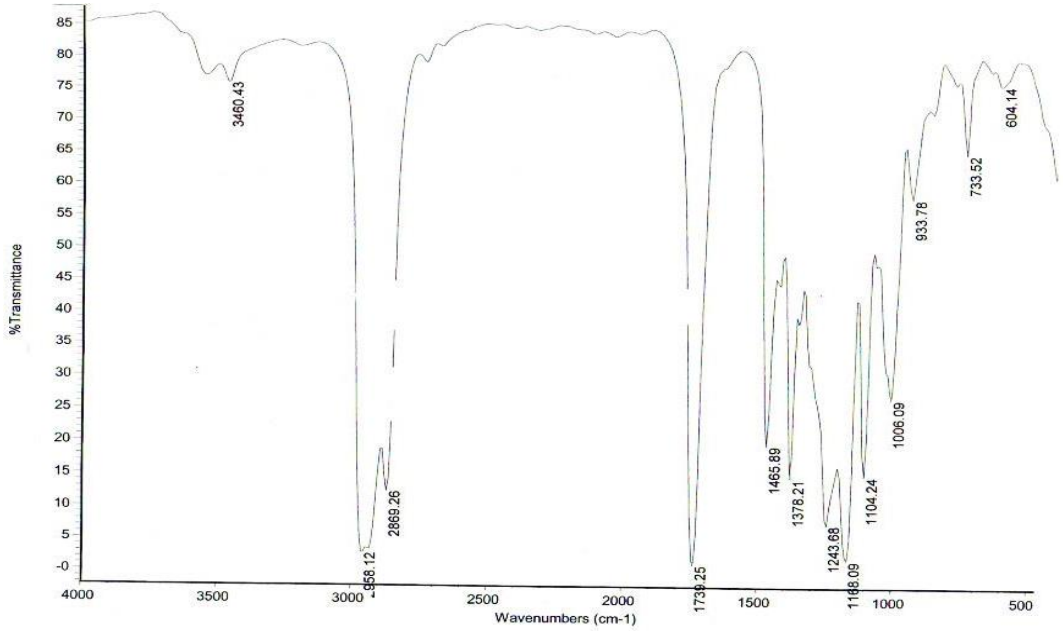

Scheme 5. FT-IR Spectrum of Neopenthylglycoldicaproate ester

Its FT-IR showed strong absorption at 1739 cm^{-1} due to carbonyl groups.

Table 3. Reaction conditions and conversions of esterification reaction using sulfated ZrO_2

Acid	Alcohol	Catalyst %	lcoholA/acid	Reactio Temperature(°C)	Reaction time (min)	Conversion[d] (%)
5[a]C	ethylenglycol	3.3	3.1	100-180	105	96
C6[b]	ethylenglycol	3.3	3.1	110-190	125	98.1
C6	ethylenglycol	3.3	3.1	100-200	130	96.6
C7[c]	trimethylolpropan	3.3	3.1	110-190	105	98.8

[a]Pentanoeic acid

[b].hexanoic acid

[c]heptanoic acid

[d] Calculated based on acid number

Conclusion

Esterification reactions of Neopenthylglycol by caproic acid in the presence of solid acidic catalysts have been investigated under solvent-less condition. The results were compared with the case of homogeneous catalyst, p-toluene sulfonic acid. Sulfated zirconia was showed the best reactivity and efficiency among the investigated heterogeneous catalysts. Effectiveness of the sulfated zirconia in the preparation of important ester compounds, which have found wide applications as plasticizer and ester base fluids, e.g. ethylenglycol, and trimethylolpropane esters was also investigated.

Using of these catalysts make the industrial processes easier, cleaner, and less complicated. The reaction work-up is also simplified. These catalysts are environmentally friendly and cleaner than conventional homogeneous catalysts, because they do not need solvent and they have very low waste. These parameters also make them economically preferred.

Acknowledgment

We are grateful to the research council of Urmia University for support of the present work.

eferences

[1]. MantriK., Komura K., Sugi Y, j.*GreenChem*, 2005, **7**, 677.

[2]. Zhao Z. H., Wang Y. Q., Nat. Sci. *J. Hunan Normal Univ*, 1990, **1**, 61.

[3]. Zhao Z. H., and Zhang. M. *CuihuaXuebao*, 1991, **12**, 328.

[4]. Zhao Z. H., Zhao R. L., Jiang S. F. *CuihuaXuebao*, 1992, **13**,237.

[5].Zhang M.,*CuihuaXuebao*, 1991,**12**: 328.

[6]. Zhao Z.H., Zhao R.L., Zhao S.F., CuihuaXuebao, 1992, **13**:237

[7].Zhao Z.H., Zhao Z.R.L., J. *Hunan Normal Univ* , 1993, 4,332.

[8].Hashimoto C., Okuhara M. T., J. *Catal*, 1993, **143**, 43.

[9].Kasai A. M., Okuhara T *ShokubaiCatalyst*, 1980, **22**,22.

[10].Yamada T., *Peterotech (Tokyo)*, 1990 , 13, 627.

[11].Okuhara T, Nishimura T., Ohashi K., Misono M., *Chem. Lett,* , 1990 **, 3**, 1201.

[12].Okuhara T, Nishimura T., Ohashi K., MisonoM., *Chem. Lett*, 1995,**4**,155.

[13]. Tonomura A S., Yamamatsu S., Adv. Technol, 1990, **2** ,127.

[14].Thora T.S, Yadav V.M., Yadav G.D., *Appl. Catal*. A**:** 1992,**90**, 73.

[15]. MohammadpourAmini M., Abedini M., Nemati A., Alizadeh M.ArabiM, J. *Mol. Catal*. A: Chem, , 1996, 114, 299.

[16].Zhao Z.H., Zhao R.L., *Zeolites,* 1993 , **13**,634.

[17].Zhao Z.H, J. *Mol. Catal.* A: Chem 2001, **168** , 147.

[18].Song T, Sayari A., *Catal. Rev. Sci. Eng*,1996, **38**,329.

[19].Corma A., *Chem. Rev*. 1997, **97**,2373. .

[20]. Mishra H.K. , Dalai A.K., Dasi D.D., Parida K.M. , Pradhan N.C., J. *Colloid Interf. Sci* . 2004, **272**, 378.

[21]. Stevens R.W., Chuang S.S.C.,*ThermochimActa*, 2003, **61**,407.

[22].Sejidov F., Mansoori Y., Goodarzi N., *Journal of Molecular Catalysis* A: Chemical,2005,**240**,186.

Communications In Catalysis
Vol. 1, No. 1, 2024, pp.20-31
DOI: 10.22049/cic.2018.13718

Azarbaijan Shahid Madani University

Using Of Ozonation Method for Filtertion of Mineral Water

HASAN ZHYAN[a*], NADER NOROOZI PESYAN , HADI JABBARI[b]

[a]Department of Organic Chemistry, Faculty of Chemistry, Urmia University, 57159, Urmia, Iran

[b]Department Of Chemistry, Payame Noor University, PO BOX 19395-4697 Tehran, Iran

Email: hassan.zhian@gmail.com

Received: 2024-03-02, Revised: 2024-03-22, Accepted: 2024-03-30

Abstract

In this reseach, two samples of mineral water found in Northern Mahabad, west Azarbaigan, with hardnesses of 36, 42 mg/l ($CaCO_3$) are investigated (.Kanisepi South Region, and Minerals of the Tutankhach Village Northern Region).
Then, different amount of Ozone gas is injected into mineral water and biological and chemical changes are observed.The used Ozonator can produce 25 mg Ozone per hour. To determine the amount of Ozone gas. We used iodometry method. By injection of 1.25 mg/l we achieved complete removal of diatomaceae in sample **1** and up to 99 percent in sample 2. Both complete removal of chlorophyceae in 1.1 mg/l complete removal of BOD_5 sample **1** in 1.1 mg/l Ozone and in sample (2 in 1 mg/l Ozone complete removal).We had 65 percent reduction of COD by injection of 1.2 mg Ozone for sample **1** and 68 percent for sample **2**.Complete disinfection is done in both samples by injection 0.5 mg per liter. In this method clean water is achieved because no chemical is used and we don't need to provide chemicals. So, Ozonation can be introducd as the best method for filtration of water.
DO: Dissolved Oxygen
BOD: Biological Oxygen Demand

COD: Chemical Oxygen Demand

Keywords: Ozonation, Filtration, Disinfection, Mineral water, clean water.

Introduction

Water is one of the most significant compounds in the life of all living beings. The human being, for example, may survive up to three weeks without eating and in moderate climates may tolerate three days of a water free life. It is therefore that water is among the essential needs for the survival of the living beings and its protection and maintenance is necessary. Undoubtedly, the access to clean water is required. Although there are abundant water resources on the planet, not all of them are usable for human beings. One of the problems in this regard is that water is not merely used for drinking. For instance, it is applied as a suitable detergent and an industrial solvent. This may lead to the pollution of surface waters. Since water resources are restricted, they should be recovered. In spite of the fact that there are more water resources in Europe than most other places in the world, the Europeans make serious efforts to treat and recover these watershemical precipitation, coalescence, inverted osmosis and adsorption was used for water treatment. Application of these methods did not result in the total removal of pollutants.

In fact, these pollutants are moving from solid to liquid and liquid to liquid phases and they may not be easily separated from water, since some of them may even have some reactions when exposed to water. Coalescence, filtration, and chlorination may really destroy microbic ingredients. However, organic destructive materials resulting from industrial sewages may exist in water. In the 1980's, it was found that the increase of chlorine in the sewages containing chain of organic materials create cyclic compounds and increase the pollution scale. Taking into account the above facts, it is mentionable that the drinking water resources are not very expensive [1].

One of the most useful methods for the destruction of pollutants in the world is the use of chemicals with high oxidation powers. Chlorine and different* compounds, electro oxidation, coalescence with electricity or ultraviolet light and different peroxides are some strong oxidants. All these materials convert insoluble organic compounds to soluble forms and even proper quantities of water and carbon dioxide may be obtained through these reactions. The result of each reaction is the oxidation of organic materials. Due to their stability and resistance to oxidation, some of these materials may be converted to smaller stable compounds. Consequently, different water treatment stages are required for enhancement of water quality. One of the most significant issues regarding the oxidition materials is that they should not be pollutant themselves. Now that water is extensively used in intensively populated areas, inorganic waters in remote places are seriously taken into account. Due to long distance of these waters from the urban and industrial centers, they may be used only after filtration and disinfection. These waters, however, may be exposed to serious threats from the pollutants. The final

solution is thus treatment and control polluted waters with a safe and proper method [2].

Results and discussions

In this research, the effects of ozone on the inorganic waters around Mahabad are examined for biological and chemical purposes.

1.The impact of ozone on the removal or reduction of biochemical oxygen demand (BOD)
2.The impact of ozone on the removal or reduction of chemical oxygen demand (COD).
3. Effects of ozone on the algae existing in mineral waters.
4. Effects of ozone on the reduction of microbial ingredients of mineral waters.
5. In this study, an ozonator with the production capacity of 25 mg of ozone per hour was used. Two springs of mineral water with the relative hardness of 36 & 42 mg/liter were used for this purpose (since they change in different seasons of the year) [3].

The use of ozone gas has a history of half a century. Ozone was first discovered by Schonbein in 1840 through the electrolysis of sulfuric acid. It was first used by Martenec in 1886 for disinfecting water. Before the mass production of chlorine gas and the examination of its biochemical and chemical properties in World War 1, Ozone was used in refining the sewages. Ozone was replaced by chlorine, following the emergence of chlorine gas since cholrine was relatively cheap and easly accessible. In the1980's, it was found that chlorine gas converts chained compounds to cyclic ones. This problem led to the return to ozone-based method. Its reliable application resulted in the discovery of other applications of ozone for the oxidation of quite dangerous metals iron and manganese in drinking waters [4].

Ozone Properties

Physical Properties

Ozone is a gas with 1.5 times of the Oxygen density. It is in fact one of the allotropes of oxygen and considered a poisonous gas, with a boiling point of 112^{0C} and is quite unstable. This gas is more stable in the gas from compared to its liquid state. It has no color or smell in gas state and is dark blue in liquid state [5].

Chemical Properties

Most of ozone reactions are rooted in the nucleophilic double bonds and this nucleus demand results in the ozone oxidation property. There are different mechanisms for the analysis of this gas, but it is widely acceptable that the hydroxide ion act as a catalyst in the ozone analysis in water solvent, which may be shown in the following manner:

$$O_3 + OH^- \longrightarrow O_2^- + HO_2$$

$$O_3 + OH^- \longrightarrow HO_4^-$$

$$O_3 + 2OH^- \longrightarrow O_2 + 2O^- + H_2O$$

Ozone usually absorbs the infrared visible light and absorbs the ultraviolet light in certain wavelengths of maximum 2500^{0A}.The solubility of the Ozone in water is 12 times that of the oxygen[6].

Ozone Reactions

Ozone reactions may be examined in three ways:

1. Initiators.
2. Inhibitors; and synergistic.
3. Synergists [7].

Initiators:

These compounds should be peroxide like materials, which are produced in the nature media (O_2^{2-}). Inorganic compounds such as peroxides, hydroperoxides, hydroxides and organic compounds such as formic acid may produce such materials. Ultraviolet rays may also produce such ingredients. Consequently, when it is cloudy, the skin is more prone to burning compared to sunny weather.

Inhibitors

Inhibitors are materials, which may consume hydroxyl ion and prevent the reproduction of anion peroxides. Inhibitors are materials such as secondary alcohols, which consume hydroxyl radical.

Synergists

All organic and inorganic materials, which may produce hydroxyl or anion peroxide are considered as synergists of ozone reactions. These synergists include compounds such as aryl, formic acid, and glyoxylic acid and primary alcohols [8].

Measuring the Ozone Gas

Measuring Ozone in the Liquid State

Since ozone is highly powerful oxidants, the applicable method shall be carefully selected. Otherwise, the reagents used are easily oxidized by ozone and other reagents resulted from the ozone analysis are easily oxidized. Therefore, in different analysis methods, including colorimetric or electrochemical ones, other oxidants also engage in the determination of the ozone volume in the analysis method and result in the existence of the ozone volume. In fact, the entire density of oxidants is usually measured and thus the result is much higher than the real volume of the ozone gas. Consequently, this error may be reduced by taking the following steps:

1- Sampling should be done carefully avoiding any mixtures and in closed tubes.
2- In order to prevent ozone loss, we directly add the gas.
3- The interval between sampling and measuring has to be short.
4- Since the manual work is prone to errors, the automatic tool-based methods are preferred [9].

Colorimetric Method (IndigoTriSulphate)

The above method was used by Beade & Hogen for the control of water pollution and is quite exact, selective and quick.

Peroxide hydrogen ions, manganese, chloride and products of ozone breakup and otheroxidations have less engagement in this method. The ozone volume should be selected in a manner that between 20-90 percent of the reagent is discolored. The stock solution is prepared using strong phosphoric acid and indigo potassium tri-sulphate.The said solution has a stability of four months in the darkness.

Iodometry

Iodide ion in the potassium iodide solution is oxidized with iodine. The acidity of the said solution shall be adjusted to lower than 2 for the ozone measurement potassium iodide is used. Thus, the ozone consumption amounts may be determined

since ozone releases iodine as a result of the following reaction: The iodine level is specified by the Sodium Thosolphate and the ozone volume is proportional to the released iodine volume.

$$O_3 + 2I^- + H_2O \longleftrightarrow I_2 + 2OH^- + O_2$$

$$I_2 + 2S_2O_3 \longleftrightarrow 2I^- + S_4O_6^{2-}$$

Considering the above reactions, it is possible to conduct the tests of BOD_5, COD and microbe culture to observe ozone effects on these waters. However, since the amounts of water in these springs change during the year, the ratio of required ozone gas will change, too [10].

Iodine Measurement in the Gas State

Ozone may also be measured in the gas state. However, ozone can be extracted from the solution indirectly by an inert gas. In the gas state it can be measured by absorption methods, such as UV and colorimetry. It can also bere introduced in the solution and measured by color indicators.

Ozone Production

The raw material for production of ozone is oxygen gas.The general reaction of ozone production has a negative enthalpy, which is an exothermic reaction. Every reaction, which may release radical oxygen, may have the required qualifications for the ozone gas production. The energy resources for this reaction may be found in following forms [11].

1- Electronic; and
2- Light

Ozone in Comparison to other Oxidants

Observing the application of this simple and effective compound is followed by the comparison to other oxidants. Taking into account the negative effects of chlorination, the application of ozone gas is really preferred, since higher costs of this method is compensated by the use of ozone through precipitation of iron and manganese, the control of smelling and taste, as well as its discoloration property and contribution to coalescence[12].

The ozone oxidation potential is 2.07 volts under acidic conditions and 1.24 volts in alkali conditions.

In the following table (1), a comparison is made between different oxidants.

Taking into account the above table, the ozone gas may have positive effects on water purification. According to the experimental taken from the ozone efficiency, different uses of ozone gas are mentioned hereunder:

1.Promotion of the coalescence process (since even after the ozonation, other particles exist in this state in the emulsion form and their mass is increased for clotting and since ozone has a radical reaction, loaded and ready-for-clotting particles are produced).

2. Oxidation of the organic pollutants (such as aromatic,phenyl,and different organometallic compounds such as insecticides.These compounds, are more stable since they have aromatic rings and the analysis of these materials shall be done with stronger oxidants).

1. Oxidation of pollutants with high molecular weights (these materials mainly form points and resins, whose cracking is done by strong oxidants)

2. Not straying microbes and algae (a powerful oxidant may destroy microbes and algae and destroy their structure,

which may have a significant role in disinfecting drinking waters).

3. Oxidation of inorganic ingredients, such as manganese and iron (some inorganic ingredients are soluble in water, but with the change of their oxidation state, they may be precipitated).

However, considering the type of pollutants, ozone should be introduced at a suitable time to increase its efficiency [13].

In this study, two springs in the vicinity of Mahabad were examined.

Ozonator

The ozonator used in this study may produce a quantity of 25 mg of ozone per hour. Pure oxygen is used for the production of ozone, but before the entry of oxygen to the ozonator. Silica gel is capable of drying the oxygen gas. However, the silica gel container should be occasionally changed; since the container gets saturated after a while and loses its drying property.

For the proper diffusion of ozone inside water, a diffuser is used, which is in the form of a porous stone and make the complete contact of ozone inside the water. All the joint used in this study are made of resistant glass.

Moreover, in order to measure the ozone amount, the iodometry method is used to determine the excess ozone. The remaineting ozone from the reaction is conducted to two vessels containing potassium iodide with certain thicknesses. Then by titrating potassium iodide with sodium thiosolphate, the volume of ozone used is determined.

In order to dry the oxygen gas, suitable drying filters are used and where there is a probability of the pollution of gas with the chemical compounds, filters with containing active carbon ingredients in granule form are used. Otherwise, ozone gas itself may produce pollution and more gas would be used, which leads to more errors.

Experimental

Ozone Measurement

Ozone and strong oxidants may oxidize potassium iodide in water solutions and release iodide. In this case, the released iodine may be titrated with sodium thiosolphate. The corresponding equations are given below [14].

Determination of Coliform Number

These microbes, which are called coliforms, are generally aerobics and in voluntary conditions, they are capable of being anaerobic. Coliforms are negative, spore-free and rod shaped. They may survive in suitable media containing lactose at 35^{0C} for 48 hours and produce carbon dioxide because of fermentation.

Identification and Counting of Algae

Algae are living beings with a high variety. Previously, before this wide variety was not identifiable, all these creatures were called algae. Some of these species have a maximum length of 50 meters and some of them may be seen only with microscopes with magnifying power of 100. Some of them may be examined by simple magnifiers. However, currently, allthe existing species are specified and have separate names.

COD Determination

100 ml of the sample is selected and added to a flask containing glass pearls. Then because to remove from the chloride troubles, 0.2 gr of mercury sulphate is added to the flask. After shaking, the 5 ml of the 0.25 normal solution of potassium bicarbonate is added to the flask. Then, 15 ml of strong sulfuric acid containing silver sulphateis introduced to the flask (the solution should be shaken, since the reaction is significantly exothermic, the observance of safety rules is required).

$$COD = \frac{(a-b)(N)(8000)}{C}$$

C= the sample volume in.

b= the Iron (II) sulphate and ammonia volume used.

a= volume of Iron (II) sulphate and the ammonia volume used as pilot.

N= Iron (II) sulphate and ammonia normality.

BOD_5 Determination

For determination of BOD_5 a German device is used. First, a certain volume of the sample is put in the particular vessel of the device and a soda tablet is added to it, and then the glass is capped. At the beginning, we select the zero grade for the device and put it in the incubator at a proper temperature, usually, 25^{0C}. After 5 days, the BOD_5 is recorded .

Results and Discussions

The results may be examined in three aspects:

1. Production of the ozone gas and factors influencing the optimization of its efficiency.
2. Properties of the samples under examination.
3. Results from the ozonation of samples at different temperatures.

Production of Ozone Gas and Effective Factors in the Optimization of its Efficiency

According to given the results in Table 2, the most proper rate for the oxygen gas introduction is 23 ml per second and the most proper time for the injection of ozone is between 50 to 400 seconds.The reason for selection of such a rate is that at higher rate, practically the production of ozone gas does not increase and in lower speeds, the ozone gas production shall be lowered. The reason to use 50 to 400 seconds is that outrange of this calibration curve shows a high deviation.

A reason for this may be that with the increase of oxygen gas rate, the required time for the effect of the electrical discharge on the oxygen molecules is reduced and many oxygen molecules pass the device without any change and lose the opportunity for changing to free radicals, caused by the device capacity.

Other subsidiary factors influencing the manner of ozone production are described below:

1. No vibration in the electrical current.
2. No chemical pollutants in oxygen gas.
3. No humidity in oxygen gas.
4. No change in the input gas current.

Properties of the Samples under Examination

Proper and sterilized vessels were used for sampling. After each sampling, all the vessels were completely sterilized by Iron, since the existence of any microbic

element in the vessel results in very high rates of error. Even in the sampling site, the wearing of sterilized gloves was required. However, for determination of BOD_5 and COD, the sterilization is not important, but for the sake of integration in the study and the elimination of all the error factors in different stages, the sterilized vessels were used.

The point, mentioned earlier, is related to the sample time because the environmental conditions of algae and microbes constantly change and at high temperatures, that is the hot seasons, these ingredients are quite active and in rainy months and at low temperatures, the microorganism activities are low.

Consequently, for the preparation of samples under study the samples were selected concurrently and were kept in the refrigerator to be used at the time of examination. However, the refrigerator was protecting from other factors, which increase the pollution probability on the samples.

Results from the Ozonation of Samples in Different Amounts

When there is a good weather and the temperature is mild, the growth of these particles will increase and requires to remove more ozone.

The next point is related to disinfecting these waters. Since they are found in quite outside environments, these waters provide very suitable media for the growth of microbes. Considering Tables 1&2 we understand that these waters have very high pollution and injecting of 0.4 mg per liter, they may be perfectly sterilized and their coliforms removed. For comparison of the activities of these bacteria, Tables 8, 10, and 11 are recommended. They show the amounts of BOD_5, and COD. With higher metabolisms, this particles consume more energy and it shows that the microbic activity in these waters are high. Therefore, when an increase in the BOD_5 and COD is observed, these waters are recommended to be disinfected. A look at Tables 1,2,3,4 indicates that injecting of 1 mg per liter, COD and BOD_5 may be totally removed.

Table 1. Change in COD as a result of Ozonation in sample (1)

Sample	COD(mg/l)	Amount of ozone injection(ppm)	% removal
original	13.5	––	--
1	13.48	0.25	0.14
2	11.98	0.50	11.25
3	8.98	0.75	33.48
4	8.4	1	35.55
5	6.5	1.25	51.85
6	5	1.5	62.96

Table 2.Changes in COD as a result of Ozonation in sample (2)

Sample	COD(mg/l)	amount of ozone injection(ppm)	% removal
original	11.5	--	--
1	10.8	0.25	6.08
2	9.1	0.50	20.8
3	7.8	0.75	32.1
4	6.2	1	46
5	4.3	1.25	62.6
6	3.8	1.5	66.95

Table 3. Changing in BOD_5 as a result of Ozonation in sample (1)

Sample	BOD_5 (mg/l)	amount injection ozone(ppm)	% removal
original	7.8	--	--
1	6.8	0.25	12.8
2	4.8	0.50	38.46
3	2.8	0.75	64.1
4	0.9	1	88.46
5	0	1.25	100
6	0	1.5	100

Table 4 .Changes in BOD_5 as a result of Ozonation in sample (2)

Sample	BOD_5 (mg/l)	amount of ozone injection(ppm)	% removal
original	7	--	--
1	6	0.25	14.28
2	5	0.50	28.57
3	3	0.75	57.14
4	1	1	85.71
5	0	1.25	100
6	0	1.5	100

Table 5. The specifications of biological sample of Tutankhach Village (Northern Region)

Entry	Organism	Number/liter
1	Diatomaceae	285
2	Chlorophyceae	95

Table 6. The results of bacteria experments of Kanisepi sample (South Region)

Number Coliphorm (MPN/100 ML)	14
Namber E.Coli in Sample(100ML)	3.2

Table 7. The results of bacteria experments of Tutankhach Village sample (Northern Region)

Number Coliphorm (MPN/100 ML)	14
Namber E.Coli in Sample(100ML)	3.2

Table 8. Change in COD as a result of Ozonation in sample (1)

Sample	COD(mg/l)	Amount of ozone injection(ppm)	% removal
original	13.5	--	--
1	13.48	0.25	0.14
2	11.98	0.50	11.25
3	8.98	0.75	33.48
4	8.4	1	35.55
5	6.5	1.25	51.85
6	5	1.5	62.96

Table 9.Changes in COD as a result of Ozonation in sample (2)

Sample	COD(mg/l)	amount of ozone injection(ppm)	% removal
original	11.5	--	--
1	10.8	0.25	6.08
2	9.1	0.50	20.8
3	7.8	0.75	32.1
4	6.2	1	46
5	4.3	1.25	62.6
6	3.8	1.5	66.95

Table 10. Changing in BOD_5 as a result of Ozonation in sample (1)

Sample	BOD_5 (mg/l)	amount injection ozone(ppm)	% removal
original	7.8	--	--
1	6.8	0.25	12.8
2	4.8	0.50	38.46
3	2.8	0.75	64.1
4	0.9	1	88.46
5	0	1.25	100
6	0	1.5	100

Table 11 .Changes in BOD_5 as a result of Ozonation in sample (2)

Sample	BOD_5 (mg/l)	amount of ozone injection(ppm)	% removal
original	7	--	--
1	6	0.25	14.28
2	5	0.50	28.57
3	3	0.75	57.14
4	1	1	85.71
5	0	1.25	100
6	0	1.5	100

Conclusion

High amounts of COD results in the use of ozone for the oxidation of organic materials. The process leads towards the disinfection when the natural organic material in the water is reduced or oxidized. Algae and microorganisms have a direct impact on the disinfection. Consequently, COD is one of the factors, which indicates the direct impact of ozone gas on the removal of all the pollutant materials (Tables 8, 9, 10 & 11).

BOD_5 shows the amount of oxygen used. Through the total removal of the natural compounds, in accordance to Tables 10 & 11, it may be observed that with the injection of proper amounts of ozone, BOD_5 shows a decreasing trend. However, it may be noticed that the BOD_5 changes are more severe than COD. In order to describe this fact, it is mentionable that at the beginning, the inseparable materials under oxidation arechanged to separable materials and they begin exhibiting biological activiting. They may increase BOD_5 amount and then be quickly oxidized by ozone, resulting in the reduction of the BOD_5. In order to overcom this problem, the oxidation time by ozone should be increased. The longer contact, time to the destruction of the subsidiary activity of organic compounds.

Acknowledgments

We are grateful to the research council of Urmia University and Urmia Payame Noor University for support of the present work.

References

[1].Bruno, Langlais David, Reckhow, D; Brink,R. Ozone in Water Treatment Application And Engineering. Lewis Publisher.1996.

[2].Masschelein,W.Ozonization Wastewater Treatment,Wiley-Inter Science Publication.1982.

[3].Woo Hang, Kim. Nishijimi,Wat. Pilot Plant Study on Ozonation And Biological Activated Carbon Process for Drinking Water Treatment, WAT.Sci. Tech1997, Vol. 35, No .8, pp 21-28

[4].American Water Work Association. Standard Method for the Examination of Water and Wastwater.1992. 18 th ed,U.S.A.

[5].Knocke,W.R. ET.AL.Kinetics of Iron and Manganes by Alternative Oxidants, AWWA. Research Foundation Final Report.1990.

[6].Paill, ET,H .AL. Application of Oxidation System to the Treatment of Natural Water,Ozone Sci. Engrg.1987.

[7].Knocke,W.ET,R. Soluble Manganeses Removal On Oxide-Coated Filter Media,Jour.AWWN.1989.Vol.80 No.12,pp.65.
[8].Standard Method for the Examination of Water and Wastewater.1998. 21th ed. USA.
[9].Amoore, J.E, 1990.The Chemistry and Physilogy of Order Sensitivity, Jour. AWWA.1990.Vol.78, No .3, pp.70.
[10].Glaze, W.H,ET.Evaluating Oxidants for the Removal of Model Teste And Order Compounds Form a Municipal Water Supply, Jour. AWWA.1990.Vol.87.No.5,pp .79-84.
[11].Kato, M. ET, AL.The Further Develoment in Ozone Application Technology in Potable Water, Ultaviolet or Ultra- sonic Assisted Ozonization. Water Supply .1983.Vol.6, pp. 34.
[12].Ho, Lionel. Newcombe, Gayle.Infuence of Character NOM (Natural of Ganic Matter) on the Ozonetion MIB and Geosmin.2002. WTR. RES, Vol. 36.pp. 511-518.
[13].Zhiqiao,H.;Shuang,S.;Huamin,Z.;Haiping,Y.;Jianmeng,C.,C.I.ReactiveBlack5 decolorization by combined sonolysis and ozonation., Ultrasonics Sonachem.2007.14 (3). 298304.14. Chiang Mai J. Sci. 35 (1).63-68.
[14].Uygur,A.; Kok, E.Decolorization treatments of azo dye wastewatecs including dichlorotriazinyl reactive groups by using advanced oxidation method.Color. Tech.1999. 115 (9), 350-354.

Communications In Catalysis
Vol. 1, No.1, 2024, pp.32-42
DOI: 10.22049/CIC.2018.13719

Azarbaijan Shahid Madani University

Preparation nanostructured materials By sol–gel crosslinking process inpresent N,N-dimethyl amino pyridiniumionic liquid as a catalysis

Hanie Musazade

Organic Chemistry Departement, Chemistry Faculty, Tabriz University.

To whom correspondence should be addressed:Tel: +989149002623

Received: 2024-04-04, Revised: 2024-04-19, Accepted: 2024-04-31

Abstract

Silica porous materials with use of the some of ionic liquids (ILs) based N, N-dimethyl aminopyridinium cation (DMAP) with high thermal stability was prepared.

First according to a proper sol-gel method, various RTILs with anions such as= Br, BF_4 as a new kind of recyclable templates in present of trimethoxysilane (TMOS) as the sol-gel precursor and deionized water were employed. Then ILs was removed from the silica matrix by calcination method.

The resulting gels were characterized by using thermogravimetric analysis, infrared spectroscopy. The calcined gels were analyzed using scanning electronmicroscopy and X-ray diffraction. In the continuous, reaction was fallowed under acidic conditions at temperature above the melting point of the functional IL such as; 2–ethoxyethyl-4-(N, N-dimethyl amino) pyridinumtetrafluoroborate with larger hydrophilic polar region in a so-called nanocasting sol-gel technique, that silica Nanostructured materials with highly ordered monolithic was obtained.

Keywords: Sol-Gel process; N, N-dimethyl amino pyridinium ionic liquid; Nanostructured material; Silica; Ionogel

Introduction

Silica based sol–gel technique has attracted a considerable interest because it has proven to be a convenient route for the preparation of hybrid compounds which combine characteristics of organic and inorganic components and applied widely in many fields, such as optical devices, sensor sciences and catalysis [1–3]. Sol–gel process is mild, which proceeds by hydrolysis of an alkoxide precursor and followed by polycondensation of the hydroxylated monomers to form a porous gel. Under this mild polymerization process, sol–gel hybrids could be easily produced by impregnates of organic reagents or copolymerization with the high reactivity of silanol by covalent bonding. The studies suggested that the properties of the sol–gel hybrids could be tuned by designing the sol–gel matrix with suitable materials.

Ionic liquids (ILs) are composed entirely of ions, which exist in liquid state at temperatures around 298 K and below. As a potentially environmentally benign reaction media, ILs have attracted more considerable attention for their unique chemical and physical properties, such as high thermal stability, high ionic conductivity, negligible vapor pressure and adjustability of characteristics via choice of the anion and cation combination etc [4-5].

Recently, ILs have been used in the preparation of sol–gel materials [6–13]. In sol–gel applications, ILs have served as solvents [6, 8, 12], pore templates [7, 9], drying control chemical additives [10], and possibly as a catalyst [12]. In several cases, ILs had significant effects on the porous structure of sol–gel materials [7,10,12], reduction in cracking and shrinking [10,11,14] during solvent evaporation from the sol–gel pores, and sol–gel reactionkinetics [10,12,15,16].

Based on unique properties of ionic liquid and advantages of sol–gel technique, new kind of hybrid materials that combine ILs with sol–gel appeared and had promising applications in preparation of nano-materials, catalysis and biosensor [17–22], Shi et al. also synthesized [RDMAP][X] based sol–gel hybrids material and characterized the resulting matrix representingcrack-free morphology because the viscous IL prevented the cracking of the sol–gel derived glasses [19-21].

In this work, according to a proper sol-gel method, various RTILs with various cations and anions as templates were used. (Scheme 1). And effect of the cations and anions in ILs on morphology and structure of the calcined silica Nanostructured materials investigated. We showed that these compounds not only for solvent, but also act as catalysis in sol-gel processes.

Experimental

Materials and reagents

All the chemicals used in the present work were purchased from Merck and used as received.

Measurements

Thermogravimetric analyses (TGA) of the air-dried gels were performed on a TGA/SDTABSI

thermogravimetricAnalyzer (METTLER TOLEDO). Samples were heated under an argon atmosphere on room temperature to 650 ℃ at 10 ℃ min^{-1}. X-ray diffraction (XRD) patterns were performed on a D_8ADVANCE (BRUKER axs) powder X-ray diffractometer. Diffraction patterns were recorded with Cu Ka radiation (40 mA, 40 kV) over a 2θ range of 1.2 ^{0} -15^0 at a scan rate of 2℃/min.

The calcined gels were characterized using scanning electron microscopy (SEM) (Philips XL30 S-2500), infrared spectroscopy (BRUKER PS15), infrared spectroscopy (IR) (BRUKER PS15) with a Perkin-Elmer. DSC differential scanning calorimeter at a heating rate of 10˚C/min in air.

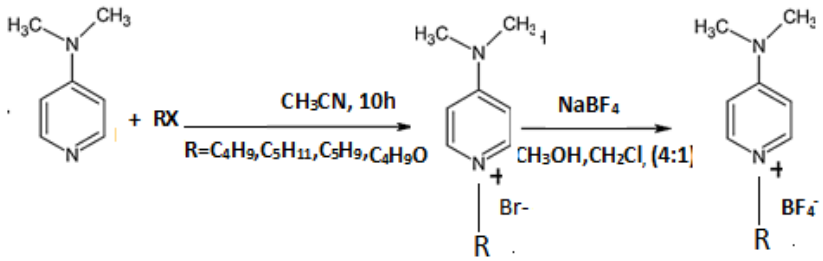

Scheme (1).Reactions processes for Ionic liquids Synthesis

Synthesis of ionic liquid compounds:

The synthetic procedure of ILsfollowed a reported route[23]. 1.22g, (10 mmol) DMAP(dimethyl amino pyridine)was added to a 50 ml three- necked round-bottom flask containing (10mmol) of anyone of compounds; 1-Bromobutane, 1-Bromopentane, 1-Bromo ethoxyethane, 1-Bromopentyne, respectively in acetonithrile and 1-Bromododecane,in dichloromethane as solvent of reaction. The mixture was heated to reflux with constant stirring for 10 h, and then cooled to room temperature. The volatile component was removed under reduced pressure to give the crude product. This compound was dispersed into ethyl acetate- isopropanol with ratio of (1:1) from which IL_nrecrystallized.

Then (10 mmol) of ILs in 10 ml dry CH_2Cl_2 was added to a solution of $NaBF_4$ (1.09g, 10mmol) dissolved in 40 ml of dry methanol. The mixture was stirred at room temperature for 20 h and then all solvents were removed. The resulting residue was dissolved in CH_2Cl_2 and it was filtered to remove NaBr, and ionc liquids of $[C_2C_3DMAP][BF_4]$,$[C_2OC_2DMAP][BF_4]$ was resulted, but $[C_4DMAP][BF_4]$, $[C_5DMA][BF_4]$was purified by column chromatography (Al_2O_3), with acetonithrile as the movable phase.

Preparation of silica Nanostructured materials with ILs ([RDMAP][X]) as the catalysis

In a typical synthesis with IL_1 as catalysis, tetramethylorthosilicate (TMOS) was used as the sol-gel precursor. Compound IL_1 (0.2 g, 1.69 mmol) was dissolved in 0.3 ml deionized water and a few minutes was heated until

60 ℃. This was allowed to cool to room temperature, then (0.625 ml) TMOS monomer was added and the mixture vortexed until a monophasic solution was obtained. Gels were stored in covered vials with punched pin-holes for a one week period to allow slow evaporation of the volatile components.

IL_1 was removed from the silica by calcinations of the sample at 550°C with a temperature ramp of 5 °C/min, and then was allowed to cool to roomtemperature with a temperature ramp of 20 °C/min. The final product was ground into a powder for further characterization. The other Nanostructured materials were prepared by repeating above procedure with the corresponding IL_s as catalysis.

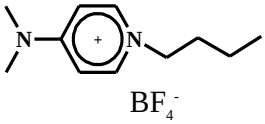

BF_4^-

$C_4DMAPBF_4$; IL_1

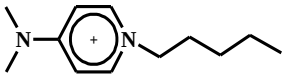

Br^-,BF_4^-

$C_5DMAPBr$, BF4 ; IL_2,IL_3

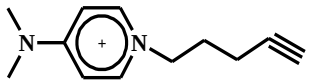

BF_4^-

$C_2C_3DMAPBF_4$; IL_4

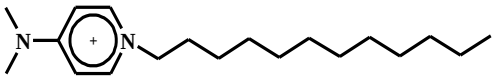

Br^-

$C_{12}DMAPBr$; IL_5

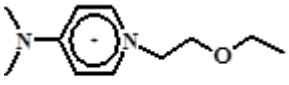

BF_4^-

$C_2OC_2DMAPBF_4$; IL_6

Scheme .2. Chemical structures of a) IL_1: 1-butyl -4-(N,N-dimethylamino) pyridiniumtetrafluoroborate($C_4DMAPBF_4$), b) IL_2: 1-pantyl -4-(N,N-dimethylamin) pyridiniumbromid and c) IL_3: 1-panty-4 -(N,N-dimethylamino) pyridiniumtetrafluoroborate ($C_5DMAPBr,BF_4$), d) IL_4 :1- pantinyl -4-(N,N- dimethylamino) pyridiniumtetafluoroborate ($C_2C_3DMAPBF_4$), e) IL_5:1-dodecyl -4-(N,N-dimehylamino) pyridiniumbromide($C_{12}DMAPBr$), f) IL_6: 2–Ethoxyethyl-4-(N,N-dimethylamino) pyridiniumtetrafluoroborate ($C_2OC_2DMAPBF_4$).

Preparation (Sg - C_2OC_2DMAP) nanocomposite under acidic condition

In this procedure 0.2g $C_2OC_2DMAPBF_4$ was mixed with 10ml of tetraethyl-orthosilicate (TEOS) and 7ml ethanol under mild magnetic stirring. After homogenization,2 ml of concentrated hydrochloride acid (36–38%) diluted by 3.5ml of distilled water was added and the mixture became coagulated gradually.After aged at 60 ℃ for 12 h, the resulted solid material was dried in

vacuum at 120℃ for 4 h. Then $C_2OC_2DMAPBF_4$ were extracted from silicamatrix by refluxing the synthesized Sg-C_2OC_2DMAP BF_4 (0.5g) in 200 mL of methanolic solution of HCl (0.5M) for 48 h.

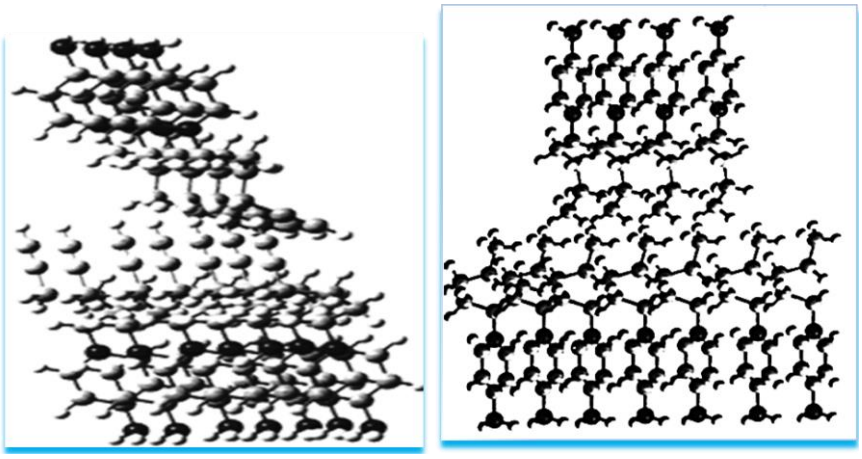

Scheme.3.tridimensional schemes of theπ -πstacking of the N, N-dimethylaminopyridinium rings and alkyl chains in pentyl and compare it with b) pentyn. (blanlk bulb is nitrogen atoms).

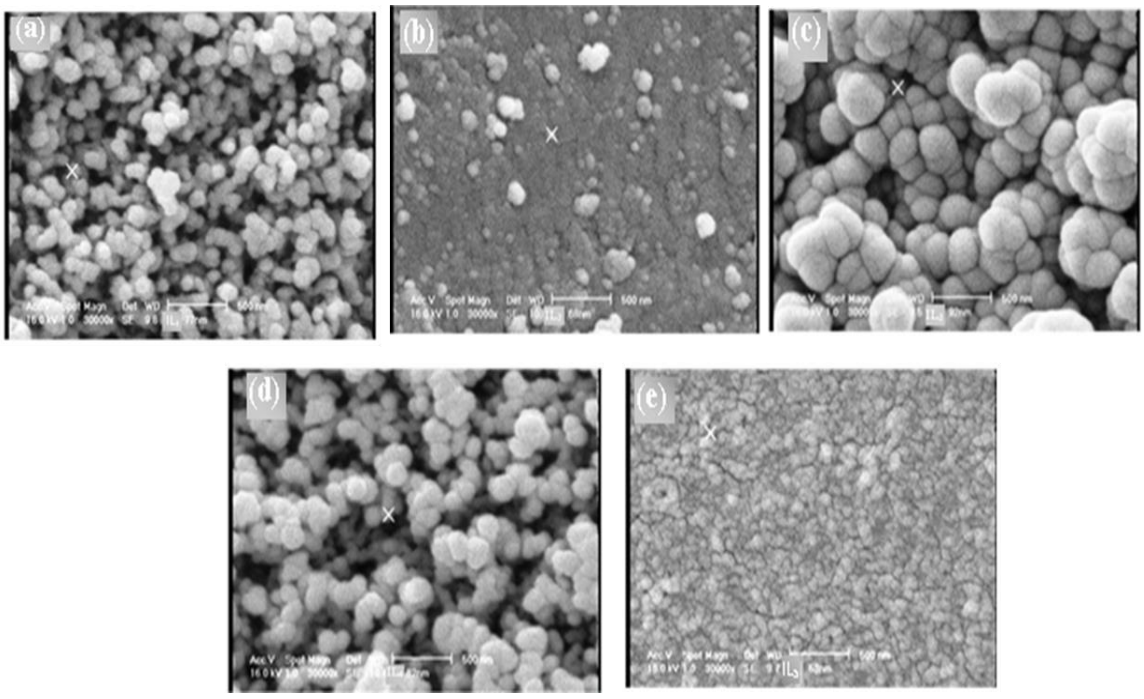

Figure (1). SEM images of the resulting morphology of the synthesized calcined silica Nanostructured materials in a molar ratio described of silicon precursor tetramethylorthosilicate to water and IL_n (n =1,2,3,4,5); scale bars: 500 nm.

Results and discussion

Some ionic liquids: ([R DMAP][X]) in which R = Bu,pentyl,), pentynyl, 2–ethoxyethyl, and dodecyl were synthesized. DMAP was reacted with alkyl bromides in which R=Bu, pentyl, pentylyl,

ethoxyethyl, and dodecyl to produce some novel ionic liquids with bromide as an anion. Then anion exchange reaction was done with some anions such as $NaBF_4$ (Scheme1). These compounds were characterized by ^1H, ^{19}F NMR and IR spectroscopic methods. The results are given below (Scheme1):

C_4DMAPBF_4 (n=1)

IR (KBr) cm^{-1} = 3030 (Ar C-H); 2932 (aliphatic C–H); 1651, 1571(Ar C=C); 726 (B-F).

^{1}HNMR (400 MHz, $CDCl_3$); δ (ppm): 0.70 (t, 3H, CH3-CH_2-); 1.09 -1.18 (m, 2H, -CH_2-CH_3);
1.59 -1.67 (m, 2H, -CH_2-CH_2-CH_3); 3.05 (s, 2×3H, CH_3-N); 4.02 (t,2H –CH_2-N); 6.7(d, 2H,
C-H Ar); 8.12 (d, 2H, C-H Ar).

^{19}FNMR (400 MHz, $CDCl_3$); δ = -152.55 ppm.

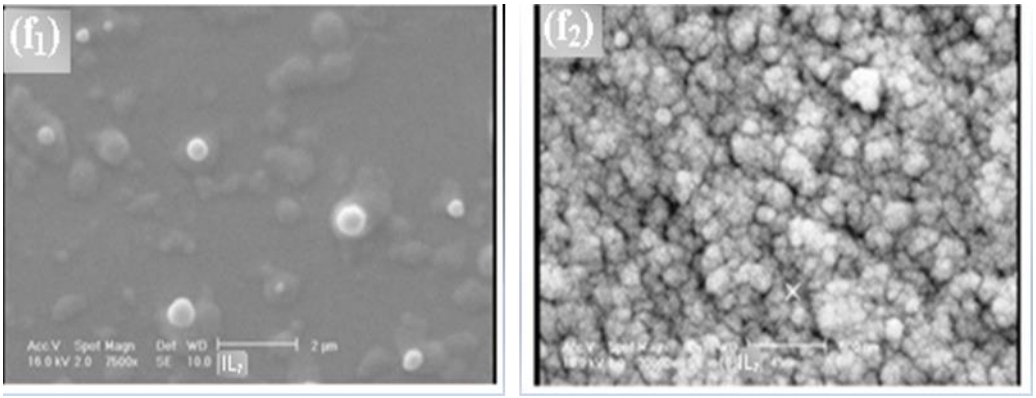

Figure(2). SEM images of the resulting morphology of the synthesized calcined silica Nanostructured materialsin a molar ratio described of silicon precursor tetramethylorthosilicate to water and IL_6(f_1) and also in present molar

ratio described of silicon precursor tetraethyl silicate to EtoH/ HCL/H_2O and IL_6 (f_2); scale bars: 500 nm.

C_5DMAPBF_4 (n=2)

IR (KBr) cm^{-1} =3015 (Ar C-H); 2932 (aliphatic C–H); 1653, 1571 (Ar C=C); 729 (B-F).

^{1}HNMR (400 MHz, $CDCl_3$); δ (ppm): 0.660 (t, 3H, CH3-CH_2-); 1.080-1.15 (m, 2×2H, - $(CH_2)_2$-CH_3); 1.64 -1.67 (m, 2H, -CH_2-CH_2-N); 3.1 (s, 2×3H, CH_3-N); 3.9(t, 2H, -CH_2-N); 6.7 (d, 2H, C-H Ar); 7.8 (d, 2H, C-H Ar).

^{19}FNMR (400 MHz, $CDCl_3$): δ = -152.91 ppm.

C_2C_3DMAP BF_4(n=3)IR (KBr) cm^{-1} = 3019 (Ar C-H); 3157 (H-C≡C); 2929 (aliphatic C–H); 1977(C≡C), 1654, 1549(Ar C=C); 770(B-F).

^{1}HNMR (400 MHz, $CDCl_3$); δ (ppm): 1.9(t, 2H, -CH_2-CH_2-N); 3.1 (s, 2×3H, CH_3-N); 4.2-4.3(t, 2H, -CH_2-N); 4.9(t, 2H, -CH_2-C≡C); 5.6-5.7 (m, 1H, H-C≡C); 6.9(d, 2H, C-H Ar); 8.4 (d, 2H, C-H Ar).

^{19}FNMR (400 MHz, $CDCl_3$); δ = -152.57 ppm.

$C_2OC_2DMAP\ BF_4$ (n=4)

IR (KBr) cm^{-1} = 3085(Ar C-H); 2932 (aliphatic C–H); 1649, 1571 (Ar C=C); 1118 (C-O); 567(B-F).

^{1}HNMR(400 MHz, $CDCl_3$); δ (ppm): 0.9(t,3H,CH_3-CH_2-); 3.3(s, 2×3H, CH_3-N); 3.33-3.38(q, 2H -O-CH_2-CH_3); 3.7(t, 2H,-CH_2-N); 4.4(t, 2H, -O-$\underline{CH_2}$-CH_2-N); 6.8(d, 2H, C-H Ar); 8.4 (d, 2H, C-H Ar).

^{19}FNMR (400 MHz, $CDCl_3$); δ = -152.46 ppm.

$C_{12}DMAPBr$ (n=5)

IR (KBr) cm^{-1} =3011 (ArC-H); 2916, 2849(aliphatic C-H); 1653,1570 (ArC=C).

^{1}HNMR (500 MHZ, $CDCl_3$); δ(ppm): 0.92(t, 3H, CH_3-CH_2-); 1.2-1.3(m, 16H, -CH_2-CH_2-);

1.8-1.9(m, 4H, -$\underline{CH_2}$-$\underline{CH_2}$-CH_2-N); 3.2 (s, 3×2H, CH_3-N); 4.3(t, 2H, CH_2-N); 7(d, 2H, C-H Ar); 8.4(d, 2H, C-H Ar).

In the next step by using these novel ILs sol-gel process were done (Scheme4). This process was started with TMSO, H_2O, and ILs.

Table.1.Characterization of thermal stability silica Nanostructured materials; $T_{g\ is}$ temperature decomposition of the ILs. Sg: Sol-gel;[RDMAP]: R=$C_{4,\ C5,\ C12}$,C_2C_3, C_2OC_2; [X]= Br, BF_4

Sg –[RDMAP][X]	**Tg (°C)**
Sg - C_5DMAP Br	358
Sg - C_4DMAP BF_4	420
Sg - C_5DMAP BF_4	438
Sg - C_2C_3DMAP BF_4	412
Sg - C_2OC_2DMAP BF_4	368
Sg - C_{12}DMAP Br	460

Characterization of gels

SEM characterization of calcined silica Nanostructured materials

Figure (1) shows the the SEM images of the resulting calcined silica Nanostructured materials froma molar ratio described of silicon precursor tetramethylorthosilicate, water, and ionic liquid based N,N-dimethylaminopyridinium cation for (a) IL_1, (b) IL_2, (c) IL_3, (d) IL_4, (e) IL_5, (f) IL_6. The ILs was used as a template in a traditional manner. SEMs of the gels revealed a mareked effect as the structure of IL was changed. Also these images show that the average particle size is below 100 nm.

Naught observation of particle in image of (f_1) relatead to hydrophilic polar region of IL_5 ; $C_2OC_2DMAPBF_4$, with the ether moiety close to the N,N- dimethyl aminopyridiniumgroup, is significantly larger of others. And as a result, increase the polar region of ionic liquid increase percent hydrogen bonding of pyridinum ring with Si-OH groups. That was prevented the formation of Si-O-Si bonds from condensation polymerization pathway. Also such hydrogen bonding would help disrupt any ring stacking compared to other ILs.Zhou et al [24] suggested a worm-hole effect (ordered periodicity) and the formation of long channels (image of a, c, d).

On the other hand performance of reaction under acidic condition, in the presence of organic solvent of ethanol and IL_6 as a catalysis and also stabilization the reaction temperature in 60$^{\circ}C$ for 12 h during the aging process, hydrolysis process accelerate, and the aging gelation was accomplished. During this period IL is molten and acts as an active supermolecule catalysis. In addition IL has a longer time for orientation porous silica framework. And as a result, silica framework was obtained with more ordered, highly porous, more uniform surface (image of f_2).

According to image of (e) in present IL_5 with long molecular chain as template; the macroporosity decreased, and a more uniform topography was observed [25]. This problem related to an increased thermal stability of IL with long molecular chain linked to N, N-dimethyl aminopyridinium cation to allow the condensation, and densification process are done in longer time in high temperatures.

In the C_2C_3DMAP BF_4 (IL4) duo to formation $\pi - \pi$ stacking pyridinium rings with pentyne alkyl chain according to Scheme (2), a ununiform morphology, size and shape was obtained(image of d).

X-ray diffraction data of calcined silica Nanostructured materials

XRD spectrum in (Fig.3) do not show any clue for the formation of crystallized silica, indicating that the silica gel materials obtained in the presemce of IL_n based N,N- dimethyl aminopyridinium cation as template are amorphous, and even after being calcined at 550°C do not observe any peak [26]. But silica porous material that synthesized in the presence of C_{12}DMAPBr template exhibits a distinct diffraction peak at $2\theta = 2.409^0$ with the corresponding d spacing about 17.5 nm, which in good agreement with the SEM observation.

Thermogravimetric analysis of the gels

The results of thermogravimetric analyses (TGA) traces of the air-dried gels are shown in table- (1). $T_{g\ is}$ decomposition temperature of the IL as the matrix of sol gel. As a result the thermal stability ILs based N, N- dimethyl aminopyridinium cation is higher than ILs based imidazolium cation. Also the large polar region in C_2OC_2DMAP based IL, due to more hydrogen bonding with matrix silica cause higher thermal stability in silica network.

On the other hand ionic liquids of long molecular chain as template was obtained micellar and packing structures from silica sol gel materials and remove this ILs was achived in higher temperatures according with result of table(1). Also exchanging anion from Br to BF_4 was increased thermal stability, that attributed to the $\pi - \pi$ stacking of the pyridinium rings and formation of hydrogen bonding between the tetrafluoroborate anion and the hydroxyl groups of the silica. The schematic illustration of the mechanism is presented in the Scheme (2), that indicates $\pi - \pi$ stacking of the pyridinium rings is more efficient than stacking of the imidazoliumrings.

Invistigation of Infrared spectroscopic characterization

Infrared spectroscopy of the non-calcined gels (Fig. 4-a) showed small peaks at areas 2900 and 2800 cm^{-1}, corresponding to the N,N-dimethylaminopyridinium cation alkyl groups and any residual methoxy groups of the silica monomer. This show that in non-calcined gel, IL is in matrix. IL is blocking the complete reaction of the monomer. These peaks are presented in all non-calcined gels.But the optimum hydrolysis conditions corresponding in the acidic environment, tesespeakes are invisible (Fig. 4-c). Also, the two characteristic bands of the N,N-dimethylaminopyridinium ring around 1600-1570 cm^{-1} could not be observed in the spectra of calcined gels(Fig. 4-b).Ofcourse this bonds adsorption in hybrid C_2OC_2DMAP- Sg under

acidic condition are as one broadband, indicating that a strong interaction between the pyridinium group and the silica matrix (Figure. 4-c).

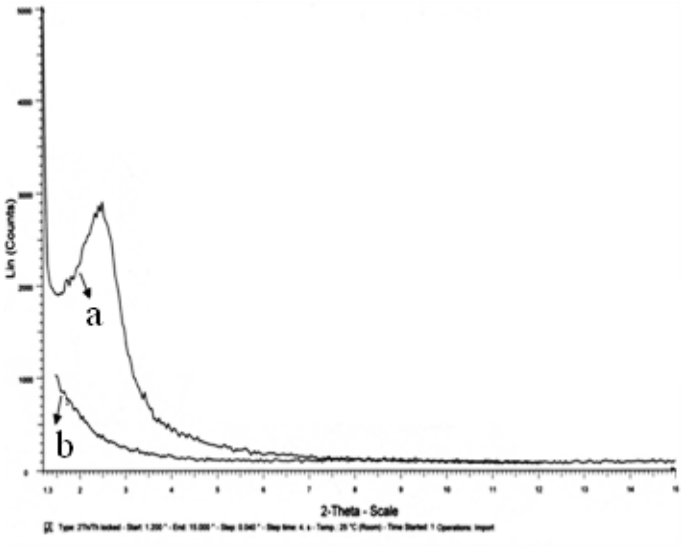

Figure (3). XRD patterns of calcined silica sol–gel materials of the(a) Sg-C_{12}DMAPBr, (b) Sg-[RDMAP][X]. [RDMAP]; R=$C_{4,\ C5,}$ C_2C_3, C_2OC_2 [X]= Br, BF_4

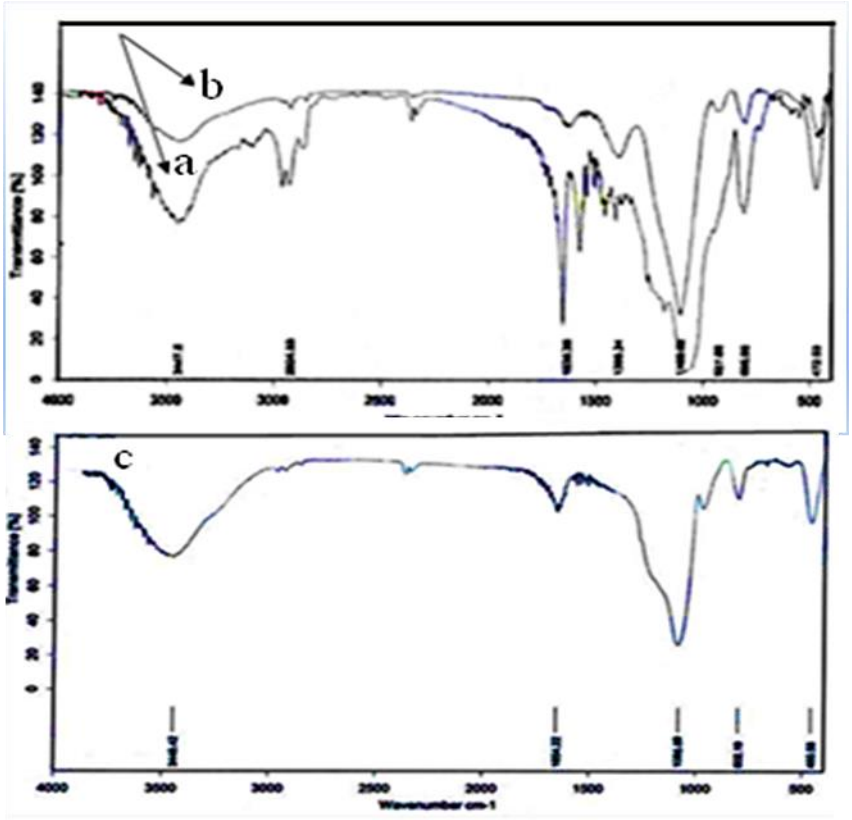

Figure (4). IR spectra of silica sol–gels: (a) non-calcined silica sol–gel; (b) calcined sol–gel synthesized with IL; (c)Sg-C_2OC_2DMAP nanocomposite under acidic condition.

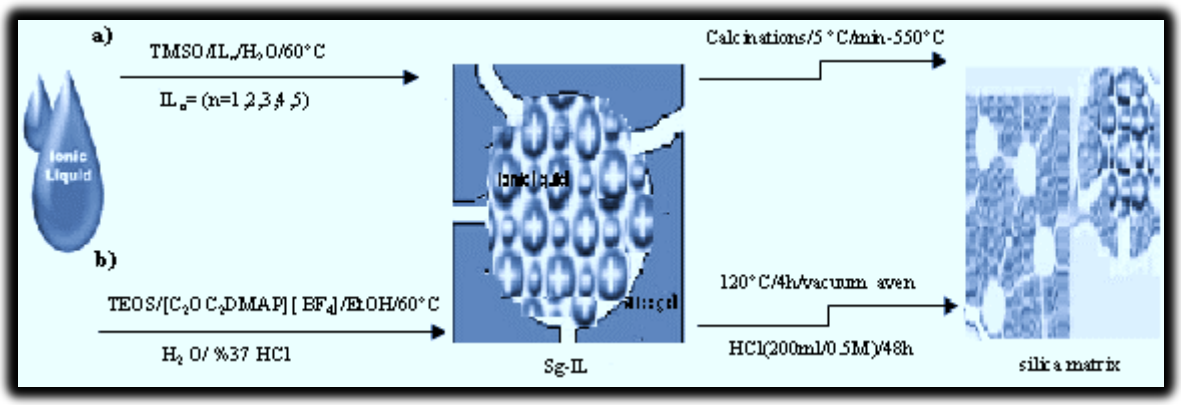

Scheme. 4-a, b.Illustration of the synthesis of silica-gel-confined ionic liquids.as catalysis: Sg:Sol-gel; IL:[RDMAP][X]:R=C_4,C_5, C_{12},C_2C_3, C_2OC_2; [X]= Br, BF_4

Conclusion

Silica Nanostructured materials with various RTILs based N, N-dimethyl amino pyridinium cation with high thermal stability as templates were synthesized according to a proper sol–gel method.

The results show that, with using various kind of ILs, various morphology, particle size, and shape was obtained. The best result was obtained in which functional ILs was used. In this case a uniform morphology, size, and shape were produced. This is especially interesting case in selective drugs loading, drugs delivery systems, and selective analytical application. In comparison hydrophilic polar region and hydrophobic region of ionic liquids C_2OC_2DMAP, C_{12}DMAPBr, as surfactant in synthesis of silica Nanostructured materials,

it was observed that with increasing hydrophobic region of IL silica frameworks with miceller and highly ordered structures was obtained. On the other hand, variety of procedure is important in synthesis, and topography of Nanostructured silica materials. In this procedure the structure of ILs important factor. And as a result of the controlled periodic porosity silica materials was obtained by using of [C_{12}DMAP][Br] as template whit long alkyl chain and also highly ordered monolithic silica Nanostructures were prepared under acidic conditions at temperatures above the melting points of the IL ([C_2OC_2DMAP][BF_4]) in a so-called nanocasting sol-gel technique.

References

[1] F. Chaumel, H. Jiang, A. Kakkar, Chem. Mater. 2001, 13, 3389.

[2] P. Gomez-Romero, Adv. Mater. 2001, 13,163.

[3] J. Wen, G.L. Wilkes, Chem. Mater. 1996, 8, 1667.

[4] J. Dupont, R.F. de Souza, P.A.Z. Suarez, Chem. Rev. 2002, 102, 3667.

[5] R. Katritzky, R. Jain, A. Lomaka, R. Petrukhin, M. Karelson, A.E.Visser, R.D. Rogers, J. Chem. Inf. Comp. Sci. 2002, 42, 225.
[6] S. Dai, Y.H. Ju, H.J. Gao, J.S. Lin, S.J. Pennycook, C.E. Barnes, Chem. Commun. 2000, 3, 243.
[7] Y. Zhou, J.H. Schattka, M. Antonietti, Nano Lett. 2004, 4, 477.
[8] Y. Liu, M.Wang, Z. Li, H. Liu, P. He, J. Li, Langmuir. 2005, 21, 1618.
[9] Y. Liu, M. Wang, J. Li, Z.Y. Li, P. He, H.T. Liu, J.H. Li, Chem. Commun. 2005, 13, 1778.
[10] M.A. Klingshirn, S.K. Spear, J.D. Holbrey, R.D. Rogers, J. Mater. Chem. 2005, 15, 5174.
[11] H.F.Wang, Y.Z. Zhu, X.P. Yan, R.Y. Gao, J.Y. Zheng, Adv. Mater. 2006, 18, 3266.
[12] A. Karout, A.C. Pierre, J. Non-Cryst. Solid. 2007, 353, 2900.
[13] H.F.Wang, Y.Z. Zhu, J.P. Lin, X.P. Yan, Electrophoresis. 2008, 29, 952.
[14] A. Safavi, N. Maleki, M. Bagheri, J. Mater. Chem. 2007, 17, 1674.
[15] K.S. Yoo, T.G. Lee, J. Kim, Micropor. Mesopor. Mater. 2005, 84, 211.
[16] H. Choi, Y.J. Kim, R.S. Varma, S. Rajender, D.D. Dionysiou, Chem.Mater. 2006, 18, 5377.
[17] M.A. Klingshirn, S.K. Spear, J.D. Holbrey, R.D. Rogers, J. Mater.Chem. 2005, 15, 5174.
[18] C.P. Mehnert, R.A. Cook, N.C. Dispenziere, M. Afeworki, J. Am.Chem. Soc. 2002, 124, 12932.
[19] Y. Liu, M. Wang, J. Li, Z. Li, P. He, H. Liu, J. Li, Chem. Commun. 2005, 1778.
[20] C.P. Mehnert, J.Chem. Eur. 2005, 11, 50.
[21] Y. Liu, L. Shi, M. Wang, Z. Li, H. Liu, J. Li, Green Chem. 2005, 7,655.
[22] F. Shi, Q. Zhang, D. Li, Y. Deng, J.Chem. Eur. 2005, 11, 5279.
[23] Y.S. Vygodskii et al. Polymer, 2004, 45, 5031–5045.
[24] Yong Zhou, Jan H. Schattka, and Markus Antonietti. J.NanoLett.. 2004, 4, 3.
[25] Yong Zhou, J.Current Nanoscience, 2005, 1, 1.
[26] J. Zhang et al. Microporous and Mesoporous Materials. 2009, 119, 97–103.

Communications In Catalysis
Vol. 1, No. 1, 2024, pp.43-57
DOI: 10.22049/CIC.2018.13720

Azarbaijan Shahid Madani University

Density functional theory study of the adsorption of toxic large molecules on nitrogen modified TiO_2 anatase nanoparticles

Amirali Abbasi, [a, b, c*] and Jaber Jahanbin Sardroodi [a, b, c]

[a] Molecular Simulation Laboratory (MSL), Azarbaijan Shahid Madani University, Tabriz, Iran

[b] Department of Chemistry, Faculty of Basic Sciences, Azarbaijan Shahid Madani University, Tabriz, Iran

[c] Computational Nanomaterials Research Group (CNRG), Azarbaijan Shahid Madani University, Tabriz, Iran

To whom correspondence should be addressed: a_abbasi@azaruniv.edu, Tel:. +984124327541

Received: 2024-04-10, Revised: 2024-05-12, Accepted: 2024-05-20

Abstract

First principles calculations were performed to study the adsorption behaviors of large organic molecules on the pristine and N-doped TiO_2 anatase nanoparticles. Both oxygen and nitrogen in the molecule can react with the TiO_2 nanoparticle strongly. Thus, the binding sites were located on the oxygen or nitrogen atom of the molecule, while on the TiO_2 nanoparticle the binding site occurs on the fivefold coordinated titanium atoms. It was found that the adsorption on the N-doped TiO_2 is more favorable in energy than the adsorption on the undoped one, indicating the high sensitivity of N-doped TiO_2 nanoparticles towards molecule molecules. It means a dominant effect of nitrogen doping on the adsorption properties of pristine TiO_2. The large overlaps in the PDOS spectra of the oxygen and nitrogen atoms of the molecule and titanium atom of TiO_2 represent a forming Ti-O and Ti-N bonds between them.

Keywords: *Molecule; TiO_2 nanoparticle; Electronic properties; Density functional theory*

Introduction

As one of the most widely studied semiconductor materials, (TiO_2) possesses various advantages in numerous applications because of its particular properties such as non-toxicity, low cost, and high catalytic efficiency [1-4]. Due to the wide band gap (3.2 eV for anatase polymorph), TiO_2 can only absorb a small percentage of the solar spectrum light (UV area). This resulted in a serious limitation of the photocatalytic activity of TiO_2. Thus, effective techniques will be needed to expand the absorption of the incoming light to the visible region. Struggles to recover the photocatalytic activity of TiO_2 catalysts to cover the range of visible light are quite prominent and indispensable. Some research studies have been devoted to the investigation of doping treatments of TiO_2 with metal or non-metal elements. In recent times, the optical sensitivity of TiO_2 was successfully improved using some of the non-metal dopants [5, 6]. This doping pattern presents energy levels in the bandgap, efficiently modifying its band energy.

Asahi and co-workers [7] exhibited that $TiO_{2-x}N_x$, in which oxygen atom was replaced by the nitrogen atom using sputtering methods, shows better photoactivity in the visible spectral range. TiO_2 has been extensively used as a suitable candidate material with a wide range of applications in photo-catalysis [8], gas sensor devices, heterogeneous catalysis [9] and photovoltaic cells [10]. Several experimental and computational studies of TiO_2 have been published, explaining its major importance in environmental remediation and toxicology reduction [11-15].

Recently, Liu *et al*. [16] reported that the N-dopedTiO_2 anatase nanoparticles can interact with toxic NO molecule more capably. Moreover, Liu *et al*. [17] studied the augmented reactivity of N-doped TiO_2 nanoparticles with CO molecules. Performing periodic Hartree–Fock calculations, Fahmi *et al*. [18] exhibited that water can adsorb on the titanium atom and then dissociate to give hydroxyl groups. Nair [19] calculated molecular and dissociative water adsorption energies on TiO_2 (001) using MSINDO-CCM (semiempirical molecular orbital method–cyclic cluster model) computations. Moreover, metal and non-metal doping of TiO_2 particles lead to some enhancements on the sensing ability and adsorption capability [20-22]. The improvements of both adsorption capability and photocatalytic activity induced by non-metal doping and other factors have been examined comprehensively [23-25]. Nevertheless, the effects of doping usage on the optical response and band gap of TiO_2 have been suggested in some studies [26-28].

Heroin molecule has been characterized as an extremely addictive drug, which is largely used by millions of addicts. Most heroin is injected, making further risks for the user, who faces the danger of AIDS or other infection on top of the pain of addiction. This molecule leads to the harmful effects on the brain cells, heart and immune system. It can increase feelings of happiness by changing activity in the limbic system. When the brain experiences such a pleasure feeling, molecule is responsible for creating

physical addiction which is typical for molecule addicts. In this work, we studied the adsorption of large molecules on the pristine and N-doped TiO_2 anatase nanoparticles. Different analyses of the adsorption configurations and systems were studied in terms of the bond lengths, density of states, molecular orbitals and Mulliken charge analysis. This work aims at investigating the effect of the doping of nitrogen atom on the electronic properties of TiO_2 nanoparticles with adsorbed molecules.

2. Details of calculations

Density functional theory calculations [29, 30] were performed with the Open Source Package for Material eXplorer (OPENMX3.8) [31]. The considered cutoff energy was set at 150 Ry in our calculations. The exchange-correlation energy was described using the generalized gradient approximation (GGA) in the formalism of Perdew–Burke–Ernzerhof (PBE) [32]. The pseudo atomic orbitals were utilized as basis sets. To completely investigate the effects of long range van der Waals (vdW) interactions, we have employed DFT-D2 method, developed by Grimme *et al*. [33]. For self-consistent field iterations, the convergence criterion of 1.0×10^{-6} Hartree was used, while for energy calculation the criterion was set to 1.0×10^{-4} Hartree/bohr. The crystalline and molecular structure visualization program, XCrysDen [34], was employed for displaying molecular orbital isosurfaces. The Gaussian broadening method for evaluating electronic DOS was used. When molecule interacts with TiO_2 nanoparticle, the adsorption energy was calculated according to the following equation.

$$E_{ad} = E_{(adsorbent + adsorbate)} - E_{adsorbent} - E_{adsorbate} \quad (1)$$

where $E_{(adsorbent + adsorbate)}$, $E_{adsorbent}$ and $E_{adsorbate}$ are the energies of the complex system, the free TiO_2 nanoparticle without any adsorbed molecule and the isolated molecule, respectively. The charge transfer between molecule and TiO_2 nanoparticle was estimated based on the Mulliken charge analysis.

We have taken the unit cell of TiO_2 from the data reported by Wyckoff [35] at the "American Mineralogists Database" webpage [36]. The size of the simulation box considered in our calculations is $20 \times 15 \times 30$ Å^3, which is much larger than the size of the particle. Two oxygen atoms of pristine TiO_2 (twofold coordinated and threefold coordinated oxygen atoms) were substituted by nitrogen atoms, leading to the N-doped nanoparticles. Twofold coordinated oxygen atom is denoted by 2f-O and threefold by 3f-O (middle oxygen) in Figure 1 with fivefold coordinated and sixfold coordinated titanium atoms sketched by 5f-Ti and 6f-Ti, respectively[37].The optimized structure of the adsorbing molecule was shown in Figure 2.

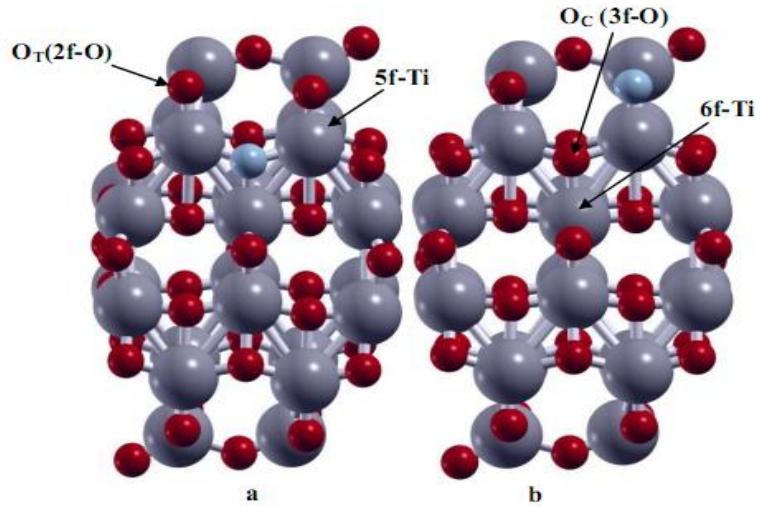

Figure 1. Optimized structures of the N-doped TiO_2 anatase nanoparticles, colors represent atoms accordingly: Ti in gray, O in red and N in blue.

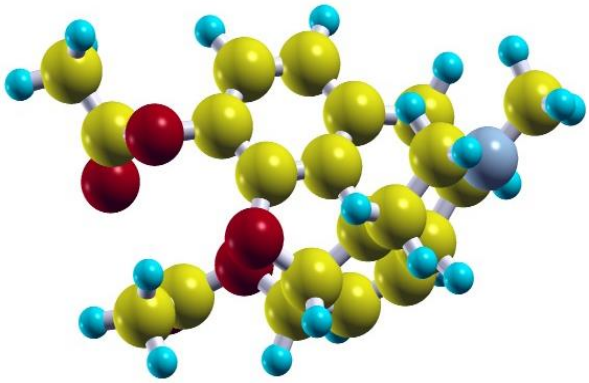

Figure 2. Optimized structure of the adsorbing molecule, colors represent atoms accordingly: C in yellow, N in blue, O in red and H in cyan.

3. Results and discussion

3.1. The interaction of molecule with N-doped TiO_2 nanoparticles

Various conformations were simulated for the pristine and N-doped TiO_2 nanoparticle + molecule, where the molecule molecule is place perpendicular to the TiO_2 surface. Three possible adsorption orientations of molecule with respect to the TiO_2 nanoparticle were considered. Important to note is that the oxygen atom in the molecule reacts with TiO_2 nanoparticle more strongly. In contrast, the nitrogen and carbon atoms do not interact with the nanoparticle. Thus, the most stable configurations of molecule adsorbed on the fivefold coordinated titanium site of TiO_2 were studied here. Optimized geometry configurations of molecule on the undoped and N-doped nanoparticles were displayed in Figures 3 and 4.

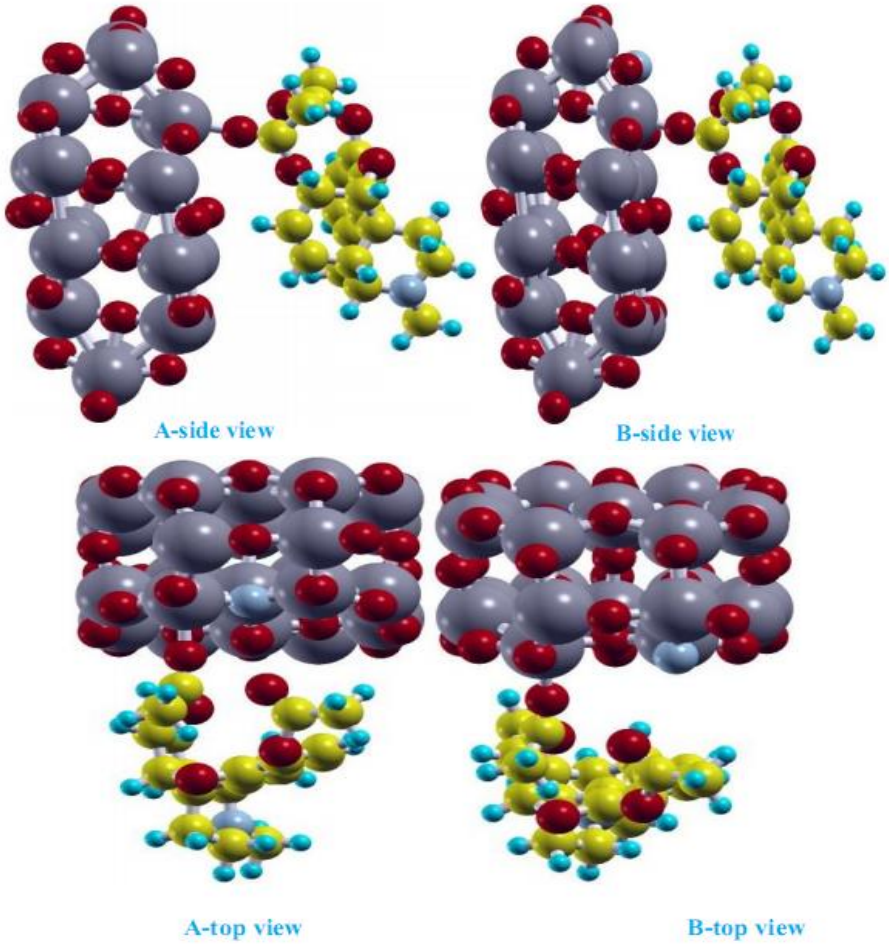

Figure 3. Optimized geometry configurations of molecule adsorbed N-doped TiO_2 anatase nanoparticles. The oxygen atom of molecule was bound to the fivefold coordinated titanium atom.

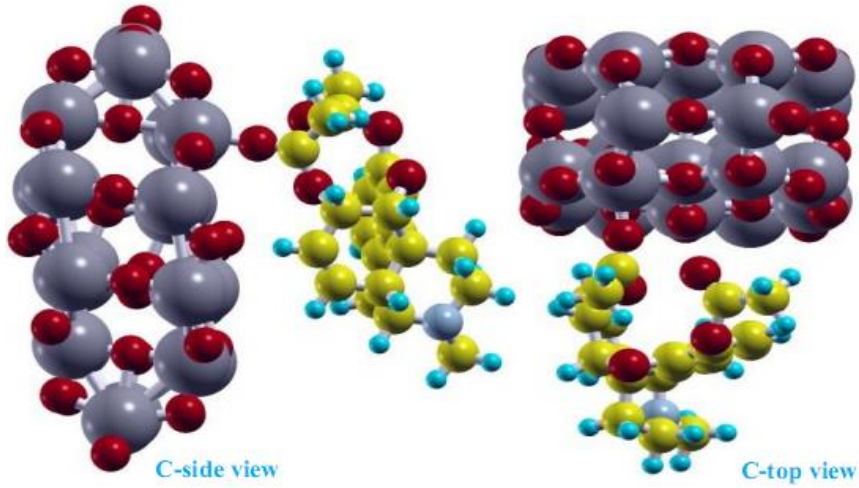

Figure 4. Optimized geometry configurations of molecule adsorbed undoped TiO_2 anatase nanoparticles. The oxygen atom of molecule was bound to the fivefold coordinated titanium atom.

These configurations were marked by labels A-C in these figures. In all cases, the oxygen atom of molecule was found to be the binding site, while on the TiO_2 nanoparticle, the binding site was located on the fivefold coordinated titanium atom.

The bond lengths for the newly-formed Ti-O bonds between the TiO_2 and molecule were listed in Table 1.

Table 1. Bond lengths (in Å), adsorption energies (in eV) and Mulliken charge values for molecule adsorbed on the TiO_2 anatase nanoparticles.

Complex	Ti-O	Adsorption energy		Mulliken Charge
		PBE	DFT-D2	
A	2.13	-4.64	-6.24	-0.612
B	2.17	-4.42	-6.14	-0.546
C	2.31	-3.82	-5.86	-0.524

For brevity, we have only reported the newly formed bonds between the molecule and nanoparticle. The smaller the distance was positioned towards the TiO_2 nanoparticle after the adsorption process, the stronger the adsorption of molecule on the TiO_2 nanoparticle. The comparison of the results presented in Table 1 indicates that the smallest distance between the oxygen atom of molecule and titanium atom of TiO_2 was occurred in configuration A, whereas the largest distance belongs to configuration C. This indicates that the strongest adsorption occurs in configuration A, representing molecule interaction with N-doped (O_C-substituted nanoparticle). In configuration C, molecule interacts with pristine nanoparticle, providing the lowest distance between the nanoparticle and molecule. By the comparison of the results, we found that the interaction of oxygen site of molecule with fivefold coordinated titanium site of TiO_2wasstrongly favored. In order to further describe the behavior of the molecule adsorbed on the TiO_2 nanoparticle, we calculated the adsorption energies of the most stable configurations (see Table 1).

The results of this table indicate that molecule adsorption on the N-doped TiO_2nanoparticle is more energetically favorable than the adsorption on the pristine one. Therefore, the N-doped nanoparticle strongly reacts with molecule. It is worth noting that the large adsorption energy gives rise to a strong binding between the TiO_2 and molecule. As can be seen from Table 1, the highest adsorption energy occurs in configuration A, representing that the interaction of oxygen atom of molecule with titanium atom is stronger than the same interaction in other configurations. The lowest adsorption energy belongs to

configuration C, which shows the interaction of pristine nanoparticle with molecule. Moreover, the adsorption of molecule on the O_C-substituted TiO_2 is more favorable in energy than the adsorption on the O_T-substituted one. By considering these results and analyzing adsorption systems, we concluded that the nitrogen modified TiO_2 nanoparticle is an ideal material to be utilized for sensing of molecule.

It should be also noted that the adsorption energies from DFT-D2 method are considerably larger than those of PBE method, representing the dominant effect of long range van der Waals interaction during the adsorption of molecule on the considered nanoparticles.

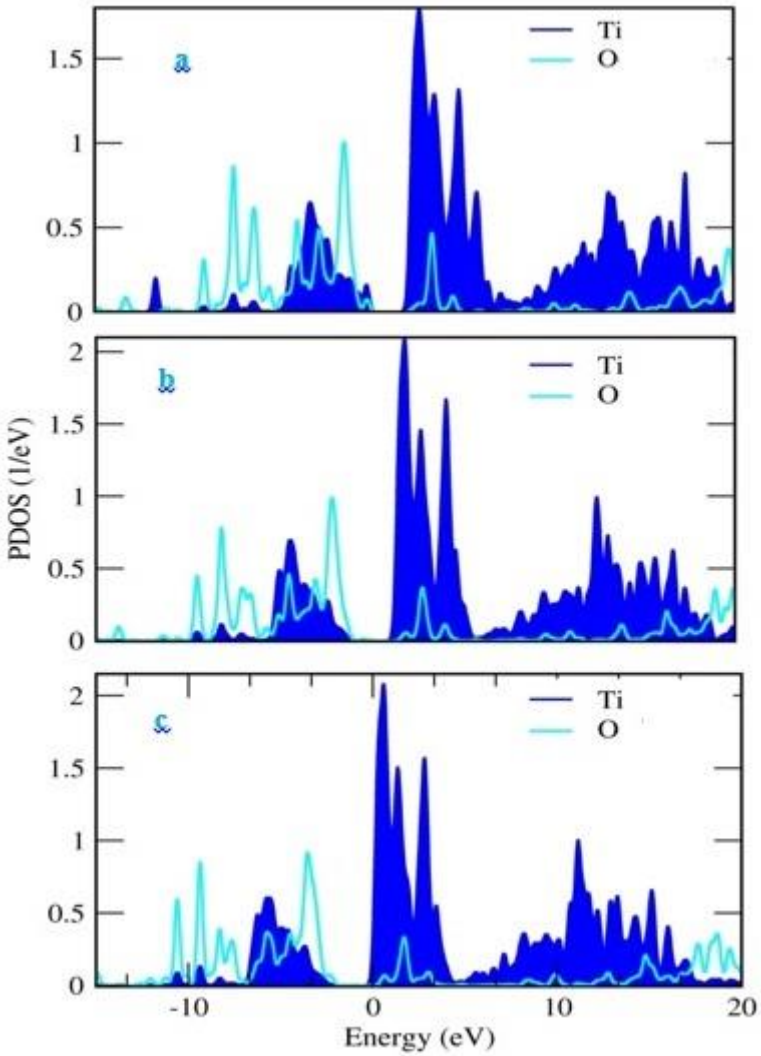

Figure 5. Projected density of states for molecule adsorbed on the TiO_2 anatase nanoparticles, a: configuration A; b: configuration B; c: configuration C.

3.2. Electronic structures

For molecule adsorption on the TiO_2 anatase nanoparticles, the projected density of states were shown in Figure 5. Panels (a-c) display the PDOSs for configurations A-C, respectively. The

considerable overlaps between the PDOSs of the oxygen atom of molecule and titanium atom of TiO_2 denote the formation of chemical Ti-O bond between them. This chemical bond formation approves the chemical adsorption of molecule on the TiO_2 nanoparticle.

As can be seen from this figure, panels (a, b) exhibit higher overlaps between the PDOSs of the oxygen and titanium atoms than panel (a), representing that molecule was strongly adsorbed on the N-doped nanoparticle, compared to the undoped one. The PDOSs of the oxygen atom of molecule, titanium atom and five d orbitals of the titanium were shown in Figures6 and 7 for configurations A and B, respectively.

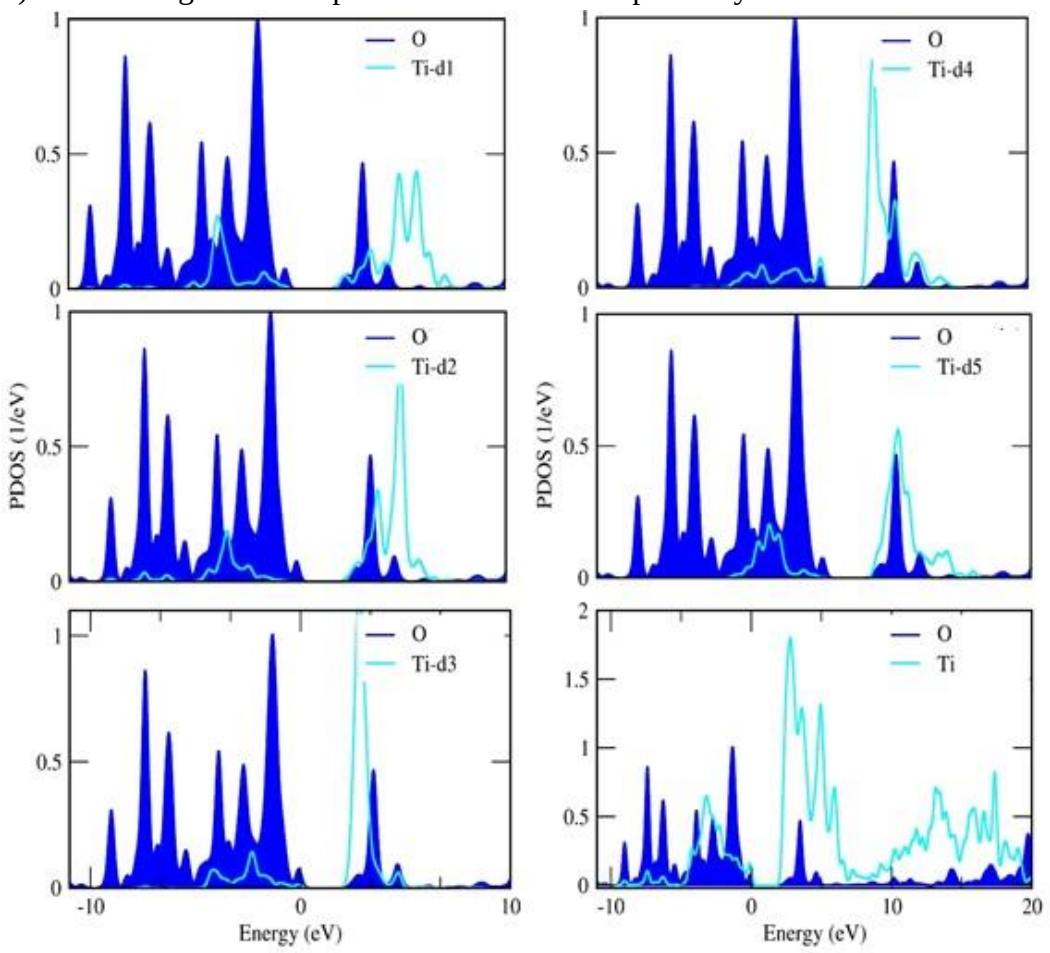

Figure 6. Projected density of states for the oxygen atom of the molecule, titanium atom and different d orbitals of the titanium (configuration A).

There are high overlaps between the PDOSs of the oxygen atom of molecule and d^2 orbital of the titanium atom, indicating effective mutual interaction between them.

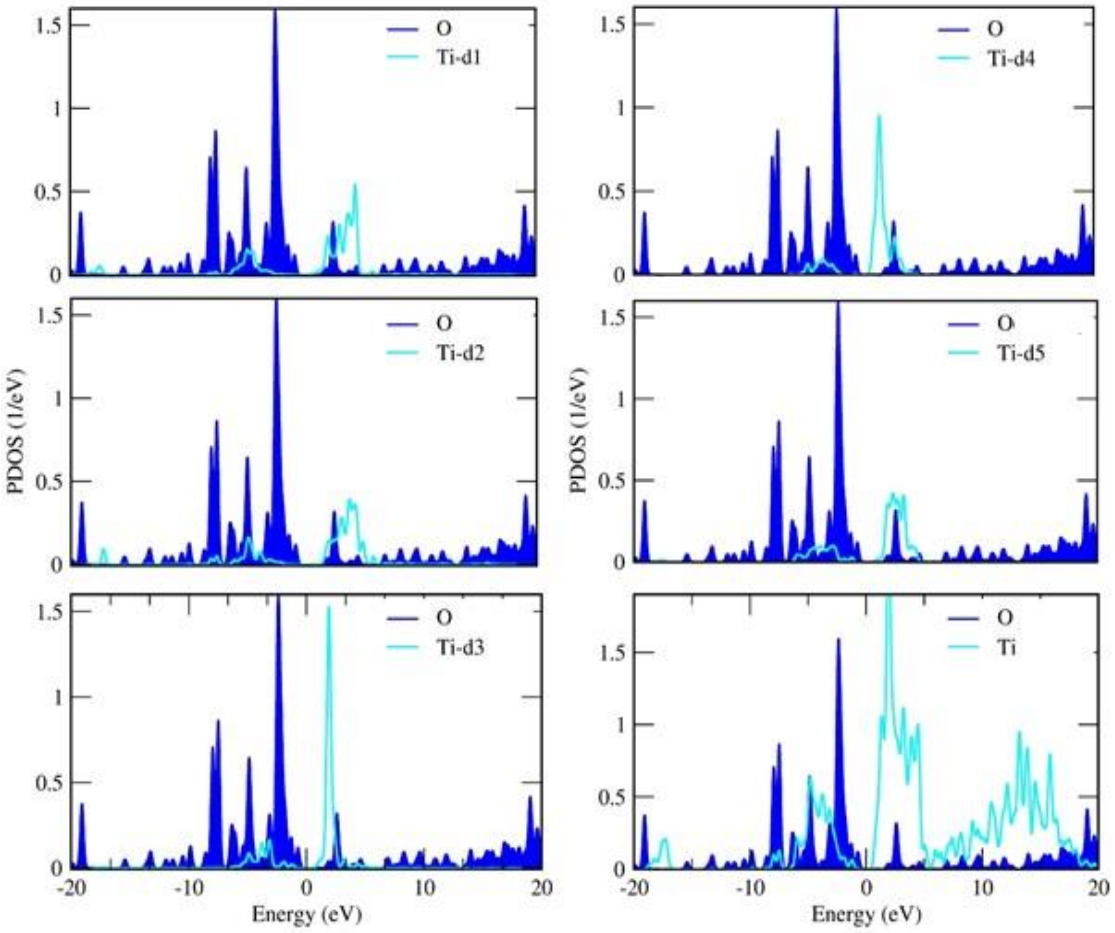

Figure 7. Projected density of states for the oxygen atom of the molecule, titanium atom and different d orbitals of the titanium (configuration B).

In order to further investigate the electronic density distribution on the TiO_2 complexes with adsorbed molecule molecules, we have presented the highest occupied molecular orbitals (HOMO) and the lowest unoccupied molecular orbitals (LUMO) for the considered systems. Figure 8 displays the HOMO and LUMO diagrams for isolated molecule.

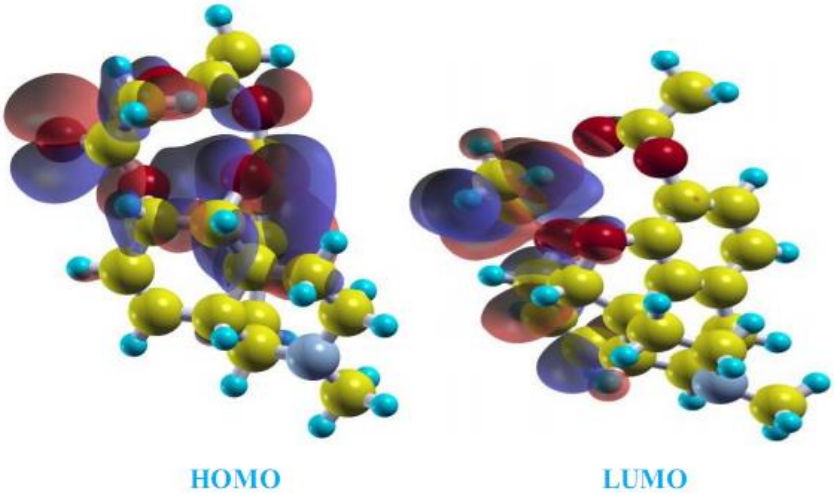

Figure 8. The isosurfaces of HOMO and LUMO of molecule in non-adsorbed state.

The HOMO of the adsorption system represents that the distribution was dominantly occurred on the whole molecule. Figures 9 and 10 show the isosurfaces of HOMOs and LUMOs for molecule adsorbed on the TiO_2 anatase nanoparticles.

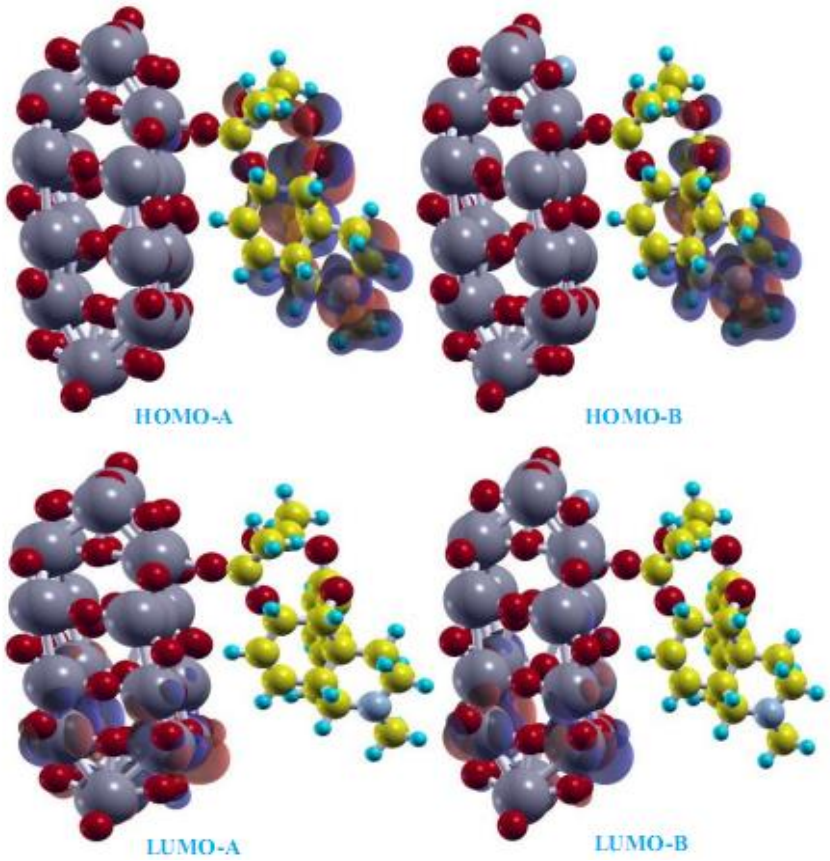

Figure 9. The isosurfaces of HOMOs and LUMOs for molecule adsorbed N-doped TiO_2 anatase nanoparticles. After the adsorption process, the electronic density was distributed over the adsorbed molecule.

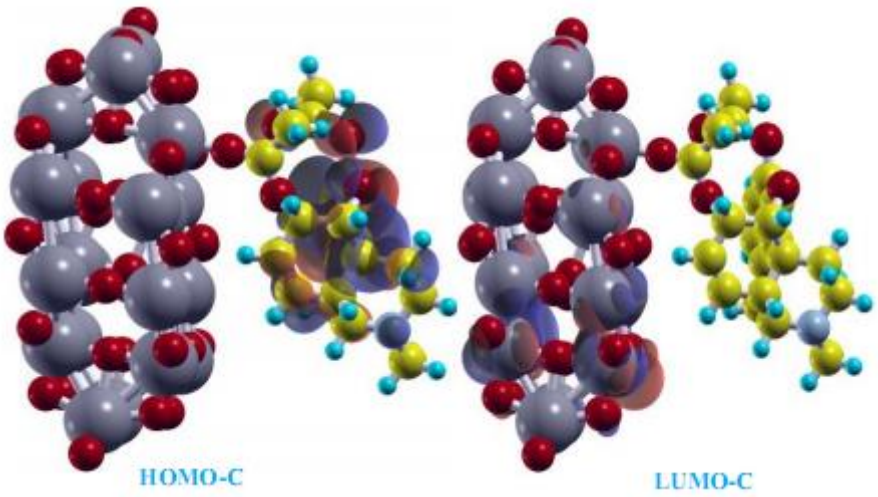

Figure 10. The isosurfaces of HOMOs and LUMOs for molecule adsorbed undoped TiO_2 anatase nanoparticles. After the adsorption process, the electronic density was distributed over the adsorbed molecule.

Interestingly, the HOMOs of the complex systems were high on the adsorbed molecule, whereas the electronic density in the LUMOs show a major distribution on the nanoparticle. Consequently, the electronic structure of the TiO_2 nanoparticle was significantly affected upon molecule adsorption. The HOMO isosurfaces of the adsorption systems indicate that the main contribution was resulted from the adsorbed molecule rather than TiO_2 nanoparticle, suggesting that molecule adsorption has substantial effect on the electronic density variation.

In addition, the charge transfer values between the adsorbent and adsorbed molecule were estimated in this work. The results were summarized in Table 1. For brevity, we have presented the charge transfer report for one configuration only. In the case of complex A, there is a considerable charge transfer of about -0.612 |e| (e, the electron charge) from molecule to the TiO_2 nanoparticle, indicating that molecule behaves as a charge donor. The maximum value of charge transfer arises from configuration A, whereas the lowest charge transfer belongs to configuration C, in reasonable agreement with higher adsorption energy of configuration A in comparison with configuration C.

The charge density difference calculations were also performed in this study in order to further examine the electronic structure of the adsorption system. It can be seen Figure 11 that the charge was dominantly accumulated on the adsorbed molecule.

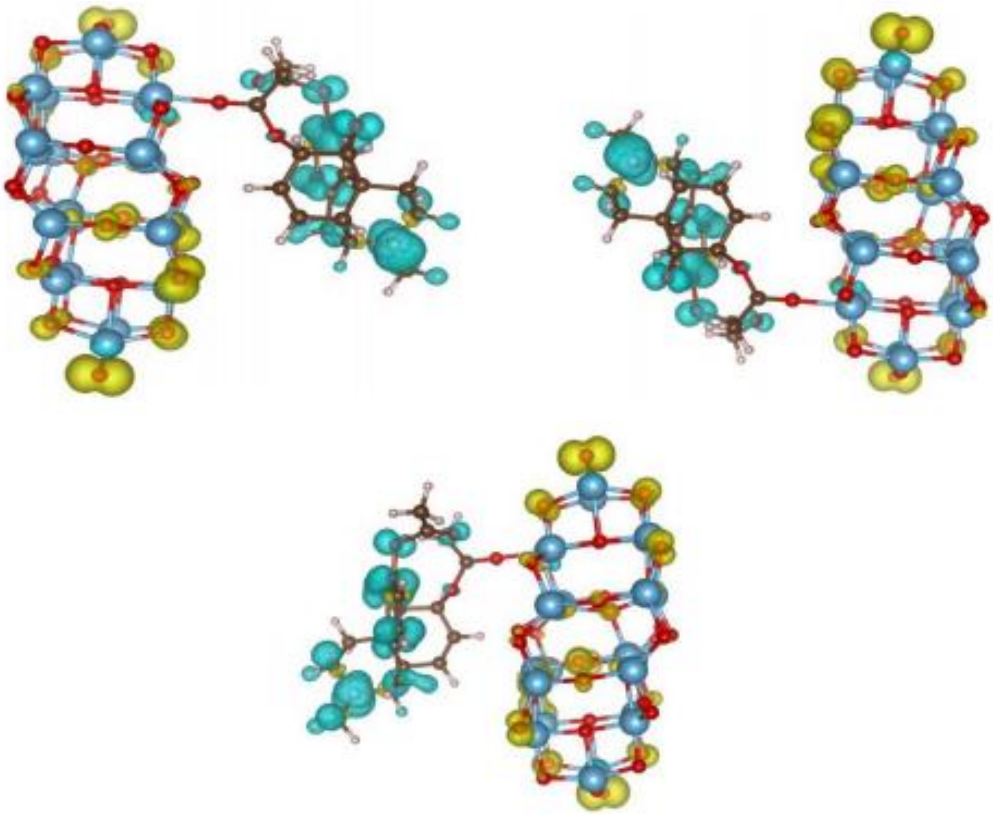

Figure 11. Isosurface plots of electron charge density difference for molecule adsorbed on the N-doped TiO_2 anatase nanoparticles.

4. Conclusions

In this paper, the interaction of molecule drug with pristine and N-doped TiO_2 anatase nanoparticles were investigated using density functional theory calculations. Various adsorption models of molecule on the considered nanoparticles were examined in detail. The calculations predict that molecule presents a stronger interaction with TiO_2 nanoparticles containing doped nitrogen atom rather than with pristine or undoped nanoparticles. The interaction of molecule with N-doped TiO_2 is more energetically favorable than the interaction with undoped ones, representing that the N-doped nanoparticle is strongly favored. By the inclusion of vdW interactions, the adsorption energies for molecule are considerably increased. The projected density of states of the oxygen and nitrogen atoms of molecule and titanium atom of TiO_2 represent considerable overlaps between these atoms and consequently formation of chemical Ti-O and Ti-N bonds at the interface region. After the adsorption, the HOMOs of the adsorption systems were mainly distributed on the adsorbed molecule. Thus, nitrogen doping into TiO_2 particle, strengthens the interaction between molecule and TiO_2 nanoparticle. The distribution of charge electron densities represents that the charges were accumulated on the adsorbed molecule.

Acknowledgement

This work has been supported by Azarbaijan Shahid Madani University.

References

[1] Linsebigler, A.L.; Lu, G.; Yates, J.T. Photocatalysis on TiO_2 Surfaces: Principles, Mechanisms, and Selected Results. J. Chem. Rev., 1995, 95: 735-58.

[2] Zhang, C.; Lindan, P.J.D.,. A density functional theory study of sulphur dioxide adsorption on rutile TiO_2 (1 1 0). J. Chem. Phys. Letts, 2003, 373: 15-21.

[3] Erdogan, R.; Ozbek, O.; Onal, I. A periodic DFT study of water and ammonia adsorption on anatase TiO_2 (001) slab. J. Surf. Sci. 6, 2010, 04: 1029–33.

[4] Hummatov, R.; Gulseren, O.; Ozensoy, E.; Toffoli, D.; Ustunel, H. First-Principles investigation of NO_x and SO_x adsorption on anatase supported BaO and Pt overlayers. J. Phys. Chem. C. 2012, 116: 6191–99.

[5] Shah, S.I.; Li, W.; Huang, C.P.; Jung, O.; Ni, C.,. Proc. Natl. Acad. Sci. U.S.A. 2002, 99, 6482.

[6] Burda, C.; Luo, Y.; Chen, X.; Samia, A.C.S.; Stout, J.; Gole, J.L... Nano. Lett. 2003, 3: 1049−1051.

[7] Asashi, R.; Morikawa, T.; Ohwakl, T.; Aoki, K.; Taga, Y. Science, 2001, 293: 269−271.

[8] Diebold, U.,. The surface science of titanium dioxide. Surf Sci. Reports, 2003, 48: 53-229.

[9] Han, F.; Kambala, V.S.R.; Srinivasan, M.; Rajarathnam, D.; Naidu, R.J. Applied Catalysis A: General, 2009, 359: 25-40.

[10] Fujishima, A.; Honda, K. Electrochemical photolysis of water at a semiconductor electrode. Nature. 1972, 238: 37.
[11] Onal, I.; Soyer, S.; Senkan, S.,. Adsorption of water and ammonia on TiO_2-anatase cluster models J. Surf. Sci. 2009, 600: 2457-2469.
[12] Shi, W.; Chen, Q.; Xu, Y.; Wu, D.; Huo, C.F., Investigation of the silicon concentration effect on Si-doped anatase TiO_2 by first-principles calculation, J. Solid State Chem. 2011, 184(8): 1983.
[13] Lei, Y.; Liu, H.; Xiao, W., (2010). First principles study of the size effect of TiO_2 anatase nanoparticles in dye-sensitized solar cell, Modelling Simul. Mater. Sci. Eng. 18: 025004.
[14] Beltran, A.; Andres, J.; Sambrano, J.R.; Longo, E.,.Density Functional Theory Study on the Structural and Electronic Properties of Low Index Rutile Surfaces for TiO_2/SnO_2/TiO_2 and SnO_2/TiO_2/SnO_2 Composite Systems, J. Phys. Chem. A, 2008, 112(38): 8943.
[15] Tang, S.; Cao, Z,. Adsorption of nitrogen oxides on graphene and graphene oxides: Insights from density functional calculations, J. Chem. Phys. ., 2011, 134: 044710.
[16] Liu, J.; Liu, Q.; Fang, P.; Pan, C.; Xiao, W.,. First principles study of the adsorption of a NO molecule on N-doped anatase nanoparticles. J. Appl. Surf. Sci. 2012, 258: 8312–8318.
[17] Liu, J.; Dong, L.; Guo, W.; Liang, T.; Lai, W.,.CO adsorption and oxidation on N-doped TiO2 nanoparticles. J. Phys. Chem. C, 2013, 117: 13037-13044.
[18] Fahmi, A.; Minot, C., A theoretical investigation of water-adsorption on titanium dioxide surfaces, Surf. Sci. 1994, 304: 343–359.
[19] Nair, N.N. Molecular dynamics investigation of clusters and solids, Ph.D. Thesis; Theoretical Chemistry Institute, Hannover University, Germany, 2004.
[20] Abbasi, A.; Sardroodi, J.J., Ebrahimzadeh, A.R., The adsorption of SO_2 on TiO_2anatase nanoparticles: A density functional theory study. Can. J. Chem, 2016, 94: 78-87.
[21] Liu, H.; Zhao, M.; Lei, Y.; Pan, C.; Xiao, W., Formaldehyde on TiO_2anatase (1 0 1): A DFT study. J Comput Mater Sci. 2012, 15: 389–95.
[22] Breedon, M.; Spencer, M.; Yarovsky, I., (2010). Adsorption of NO_2 on Oxygen Deficient ZnO (2) for Gas Sensing Applications: A DFT Study, J. Phys. Chem. C, 2010, 14 (39): 16603.
[23] Livraghi, S.; Paganini, M.C.; Giamello, E.; Selloni, A.; Valentin, C.D.; Pacchioni, G., Origin of Photoactivity of Nitrogen-Doped Titanium Dioxide under Visible Light. J. Am. Chem. Sci. 2006, 128: 15666-15671.
[24] Rumaiz, A.K.; Woicik, J.C.; Cockayne, E.; Lin, H.Y.; Jaffari, G.H.; Shah, S.I. Oxygen vacancies in N doped anatase TiO_2: Experiment and first-principles calculations, App Phys. Letts , 2009, 95 (26): 262111.
[25] Zhao, Z.; Liu, Q. Effects of lanthanide doping on electronic structures and optical properties of anatase TiO_2 from density functional theory calculations, Journal of Physics D: Applied Physics, 4, 2008, 1(8): 085417.

[26] Gao, H.; Zhou, J.; Dai, D.; Qu, Y, Photocatalytic activity and electronic structure analysis of N-doped anatase TiO_2: A combined experimental and theoretical study, J. Chem. Eng. Technol, 2009, 32: 867.
[27] Zhao, D.; Huang, X.; Tian, B.; Zhou, S.; Li, Y.; Du, Z.,.The effect of electronegative difference on the electronic structure and visible light photocatalytic activity of N-doped anatase TiO_2 by first-principles calculations, Appl. Phys. Lett, 2011, 98: 115-124.
[28] Landmann, M.; Rauls, E.; Schmidt, W.G., The electronic structure and optical response of rutile, anatase and brookite TiO_2, Journal of Physics: Condensed Matter, 2012, 24: 195503.
[29] Hohenberg, P.; Kohn, W., Inhomogeneous electron gas, J. Phys. Rev, 1964, 136: B864–871.
[30] Kohn, W.; Sham, L., Self-Consistent equations including exchange and correlation effects, Phys Rev, 1965, 140: A1133–A1138.
[31] Ozaki, T.; Kino, H.; Yu, J.; Han, M.J.; Kobayashi, N.; Ohfuti, M.; Ishii, F., et al., The code OpenMX, pseudoatomic basis functions, and pseudopotentials are available on a web site 'http://www.openmxsquare.org'.
[32] Perdew, J.P.; Zunger, A., Self-interaction correction to density-functional approximations for many-electron systems. J. Phys. Rev. B, 1981, 1396: 5048-5079.
[33] Grimme, S.,). Semiempirical GGA-type density functional constructed with a long-range dispersion correction, J. Comput. Chem, 2006, 27: 1787-1799.
[34] Koklj, A, Computer graphics and graphical user interfaces as tools in simulations of matter at the atomic scale, J. Comput. Mater. Sci., 2003, 28: 155-168.
[35] Wyckoff, R.W.G., (1963). Crystal structures, Second edition. Interscience Publishers, USA, New York.
[36] Downs, R.T., Web page at: http://rruff.geo.arizona.edu/AMS/amcsd.php.
[37] Wu, C.; Chen, M.; Skelton, A.A., Cummings PT, Zheng T. ACS Appl. Mat Interfaces, 2013, 5: 2567-2579.

Communications In Catalysis
Vol. 1, No. 1, 2024, pp.58-66
DOI: 10.22049/CIC.2018.13721
Azarbaijan Shahid Madani University

Synthesis and characterization of novel micro-sized tetrazole-based high energetic nitrogen-rich polymers

MehrdadMahkam[a], ShabnamJahanbani-Korabbaslo[b], RoghayyehFathi[b], Leila Nazmi[b], Ebrahim Rezaii[a*]

[a]Chemistry Department, Faculty of Science, AzarbaijanShahidMadani University, Tabriz, Iran

To whom correspondence should be addressed: Ebrahimrezayii@gmail.com, Tel: +989353387358.

Received: 2024-04-20, Revised: 2024-05-17, Accepted: 2024-05-31

Abstract

Energetic materials are a class of material with high amount of stored chemical energy that can be released. Typical classes of energetic materials are e.g. explosives, pyrotechnic compositions, propellants (e.g. smokeless gun powders and rocket fuels), and fuels (e.g. diesel fuel and gasoline). The novel functionality of aromatic tetrazole derivatives with high nitrogen content predetermines a great interest to tetrazole-containing polymers. The tetrazole-based nitrogen-rich polymers were well investigated. The tetrazole rings play an important role in development of energetic polymers. The high thermal stability of these rings causes the polymers as good candidates as energetic applications. The aim of the present work is to synthesize novel nano-sized high energy density polymers based on tetrazole rings. The resulted polymer was characterized by SEM, 1H NMR and 13C NMR.

Keywords: Nano-size;Tetrazole; Nitrogen-rich polymers; Explosives; Energetic materials.

Introduction

High energetic materials can be classified as three types of nuclear, physical and chemical explosives. The decomposition of compounds with production of heat and gases is the deduction of detonation process of explosives. The important groups of energetic compounds are related to the primary and secondary explosives, propellants and pyrotechnics [1-2]. From a structural point of view, the explosives can be classified as nitro compounds, nitric esters , nitramines, chloric and perchloric acid derivatives, azides [3-4] and various molecules capable of preparing a detonation (acetylides, fulminates, ozonides, peroxides and polynitrogen compounds (PNCs) such as tetrazole-, triazole-,triazine- and tetrazine-based compounds). Nitrogen-rich polymers point to the polymer structures including a high content of nitrogen atoms, frequently over 50 percent [5-6]. This high nitrogen content can be gained by the aza-based aromatic rings. Nowadays, the several high energetic nitrogen-rich polymers were developed and reported in scientific papers. Common high energetic polymers have nitro or azide groups [7]. From the most known energetic polymers, nitrocellulose (NC) [8-9], glycidylazide polymer (GAP) [10], poly[3,3-bis(azidomethyl)oxetane] (polyBAMO), poly(azido methyl methyloxetane) (polyAMMO), poly(nitrato methyl methyloxetane) (polyNMMO/polyNIMMO) [11], polyglycidyl nitrate (polyGLYN) [12] and polyvinyl nitrate (PVN) [13] can be noted. In recent years, a number of researchers work on aza-heteroaromatic ring based polymers. The tetrazole-based nitrogen-rich polymers were well investigated. The tetrazole rings play an important role in development of energetic polymers [14]. The high thermal stability of these rings causes the polymers as good candidates as energetic applications. Recently we reported some nitrogen-rich polymers: PAST1, PAST2, (PTMS), PTNSA1, PTNSA2, (PTS) and PDATS polymers. The aim of the present work is to synthesize novel nano-sized high energy density polymers based on tetrazole rings.

Experimental

Materials

The acrylonitrile, azobisisobutyronitrile (AIBN), ammonium chloride, hydrochloric acid (37%), ammonia (25%), hydrazinium hydroxide (95%), hydroxylamine (50%), aminoguanidine bicarbonate (97%), sodium azide and all solvents were purchased from Sigma-Aldrich Company. All the solvents were distilled and stored over a drying agent.

Measurements

Infrared spectra were recorded with a 4600 Unicam FT-IR spectrophotometer as KBr pellets. Nuclear magnetic resonance (NMR) spectra were run on a Bruker 400 MHz spectrometer at room temperature using deuterated solvents. The thermogravimetric analysis (TGA) and differential scanning calorimetry (DSC) curves were obtained on a TGA/SDTA 851 calorimeter at heating and cooling rates of 10 °C/min under N_2.

Polymerization of acrylonitrile: PAN

For preparing of polyacrylonitrile (PAN), the acrylonitrile (10 ml) was dissolved in 100 mL of toluene and was mixed with AIBN (1%

molar) as a radical initiator, in a pyrex glass ampoule. The ampoule was degassed under argon gas, sealed under vacuum, and maintained at 80 ± 1 ºC in a water bath, with stirring for about 24 h. The polymerization temperature was well controlled in a water bath. After reacting for 24 h, the ampoule was cooled rapidly. Then the solutions were poured into cooled methanol. The light yellow precipitates were collected and washed with methanol three times and dried under vacuum to yield (approximately 95%) of PAN (Scheme 1).

Synthesis of poly(5-vinyltetrazole): PVT

The reaction of PAN polymer with sodium azide and ammonium chloride (Scheme 2) were done in a conical bottle equipped with stirrer and reflux condenser. About 1.4 g (26.4 mmol) of PAN powder and 30 mL of DMF were added to a conical bottle with stirring at room temperature. Then to the solution, 1.68 g (25.8 mmol) of NaN_3 and 1.4 g (26..2mmol) of NH_4Cl were added with stirring. The bottle was immediately placed into an oil bath and heated to 120 ºC and maintained the temperature with stirring for 24 h. After reacting, the ampoule was cooled rapidly to room temperature. The final reaction mixture was added into distilled water for precipitate and also an elimination of DMF. The products obtained were treated in 300 mL of 0.5 M HCl and repeatedly washed with distilled water for a complete removal of Cl^-, Na^+ and H^+. The brown precipitates were left to dry at room temperature in air for several days (yield around 95%).

Synthesis of ammonium salt of poly(5-vinyltetrazole): APVT

1 g (10.4 mmol) of PVT powder, 10 mL of distilled water and 1 mL of ammonia 25% were poured in an ampoule and stirred at 35 ºC for 48 h. After this period of time, the reaction mixture was heated into the oven at 50 ºC for 24 h. The yellow precipitates (Scheme 3) were obtained. The yield of this reaction was 42%.

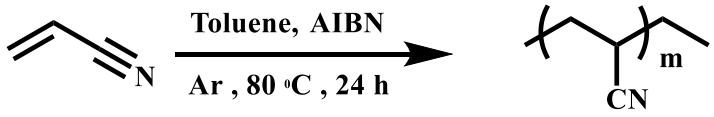

Scheme 1. Preparation of PAN.

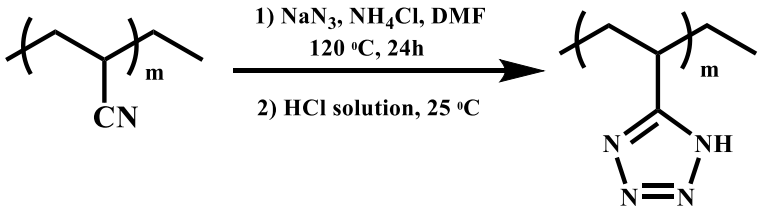

Scheme 2. Preparation of PVT.

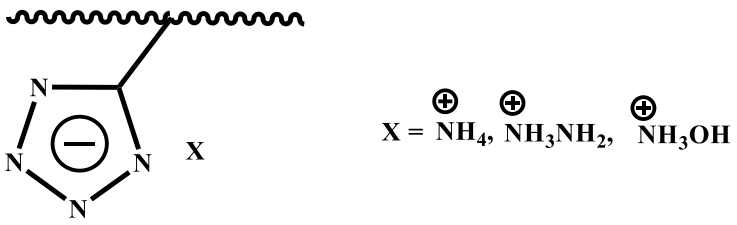

Scheme 3. Structure of PVT salts.

Synthesis of hydrazinium salt of poly (5-vinyltetrazole): HPVT

For preparation of HPVT, 1 g (10.4 mmol) of PVT powder was poured in a pyrex ampoule containing 10 mL distilled water. Then 0.51 mL of hydrazinium hydroxide was added to the mixture. All reactants were stirred together at 35 ºC for 48 h. After the reaction time, the reaction mixture was heated in the oven at 40 ºC for 24 h. The yellow precipitates (Scheme 3) were collected and weighted (approximately 70%).

Synthesis of hydroxyl ammonium salt of poly(5-vinyltetrazole): HAPVT

The nitrogen-rich HAPVT salt (Scheme 3) was obtained by the reaction of PVT powder (1 g, 10.4 mmol), distilled water (10 mL) and hydroxylamine solution (0.6 mL). All reactants were reacted at 35 ºC for 48 h with hard stirring. Then, the reaction mixture was heated into the oven at 45 ºC for 24 h. The yield of this yellow nitrogen-rich polymer was approximately 75%.

Synthesis of aminoguanidinium salt of poly(5-vinyltetrazole): AGPVT

In a two-necked pyrex glass ampoule, 1 g (10.4 mmol) of PVT powder was stirred with 40 mL of distilled water under argon gas. After the degassing of the ampoule, 0.7 g (9.4 mmol) of aminoguanidine bicarbonate was added to the reaction mixture and stirred hardly with them. After 24 h, the yellow precipitates (Scheme 4) were dried under vacuum. The yield of this reaction was approximately 70%.

Synthesis of nano-sized nitrogen-rich polymers

For preparing of nano-sized energetic polymers, the synthesized polymers (APVT, HPVT, HAPVT and AGPVT) were dissolved in distilled water and cooled in freeze-drying machine at -80 ºC for 2 h. Then, the compounds were dried in freeze-drying equipment for 24 h.

Results and discussion

The structures of the salts of poly(5-vinyltetrazole) were characterized by FT-IR spectroscopy technique. The nitrogen-rich salts were not soluble in NMR solvent. Then, the NMR analysis of the compounds was not performed. The characterizations of all synthesized compounds are drawn in below:

PAN: ^{1}H NMR (DMSO-d^{6}, ppm): 2.05– 2.09 (CH_2), 3.15- 3.19 (C-H) (Figure 1). FT-IR (KBr, cm^{-1}): 2938 (aliphatic C-H), 2243 (CN), 1454 (bending C-H).

PVT: ^{1}H NMR (DMSO-d6, ppm): 2.1 (2H, t, CH_2), 3.1 (1H, m, CH) and 7.2-7.3 (1H, s, NH) (Figure 2). ^{13}C NMR (DMSO-d6, ppm): 30 (CH_2 and CH) and 160 ($C_{tetrazole}$) (Figure 3). FT-IR (KBr, cm^{-1}): 3300-3500 (stretching N-H), 2850-3000 (stretching C-H), 1557-

1636 (stretching C=N), 1456 (bending C-H and N-H) and 1056-1355 (bending C=N).

APVT: FT-IR (KBr, cm^{-1}): 3423 (stretching N-H), 2853, 2925 and 3070 (stretching C-H), 1561-1624 (stretching C=N), 1410-1460 (bending C-H and N-H) and 1030-1245 (bending C=N).

HPVT: FT-IR (KBr, cm^{-1}): 3421 (stretching N-H), 2853 and 2925 (stretching C-H), 1543-1637 (stretching C=N), 1409-1473 (bending C-H and N-H) and 1029-1245 (bending C=N).HAPVT: FT-IR (KBr, cm^{-1}): 3421 (stretching N-H and O-H), 2925 (stretching C-H), 1542-1636 (stretching C=N), 1409-1473 (bending C-H and N-H) and 1033-1206 (bending C=N).

AGPVT: FT-IR (KBr, cm^{-1}): 3423 (stretching N-H), 2853 and 2924 (stretching C-H), 1638-1719 (stretching C=N), 1384-1459 (bending C-H and N-H) and 1099 (bending C=N).

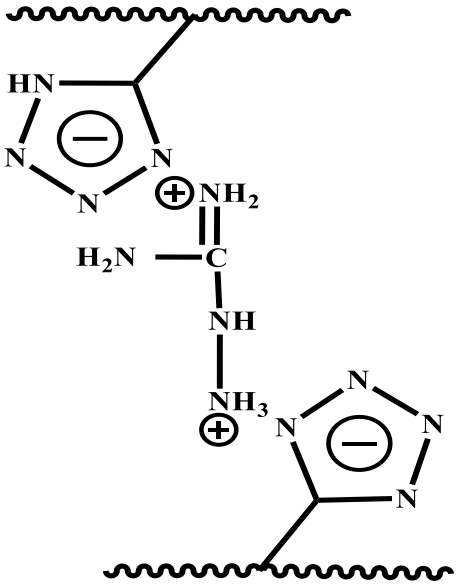

Scheme 4. Structure of aminoguanidinium salt of PVT.

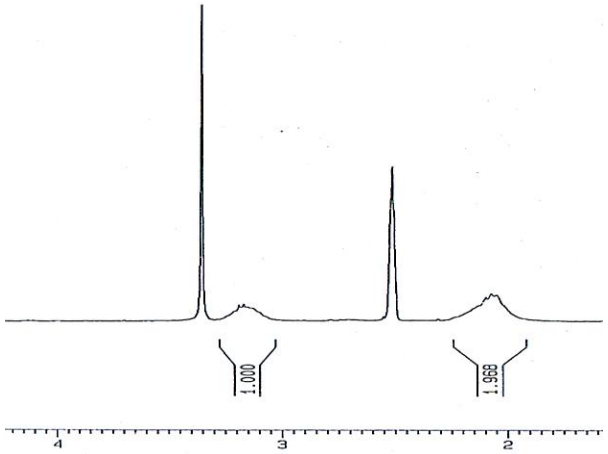

Figure 1. ^{1}H NMR spectrum of PAN in DMSO-d6.

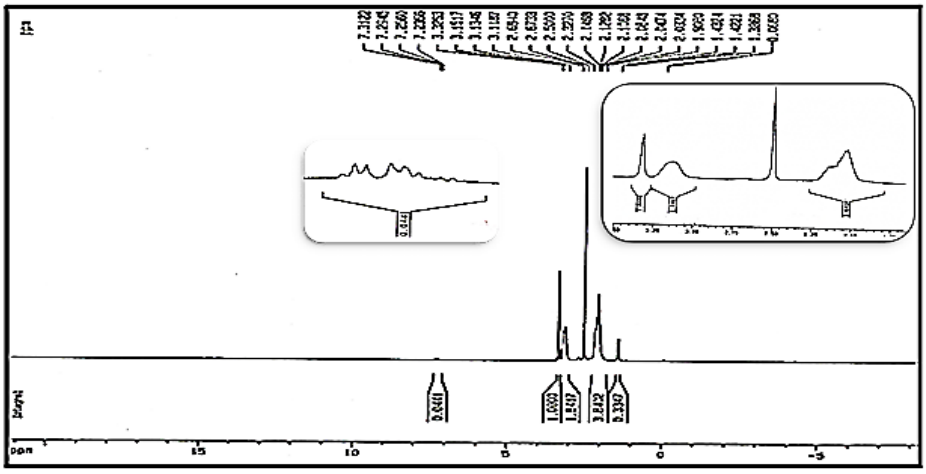

Figure 2. ^{1}H NMR spectrum of PVT in DMSO-d6.

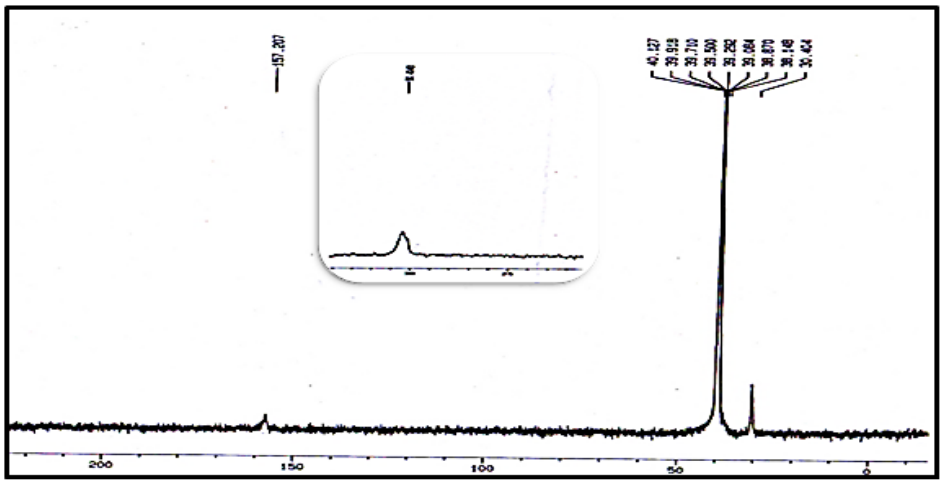

Figure 3. ^{13}C NMR spectrum of PVT in DMSO-d6.

Figures 4-7 show the SEM micrographs of the nitrogen-rich salts of the PVT. The particles sizes were 30 μm, 300 nm, 30 μm and 1 μm for APVT, HPVT, HAPVT and AGPVT salts, respectively.

Thermal properties of polymers were studied by TGA technique and were listed in Table 1. The IDT, PDT and PDT_{max} are related to the initial decomposition temperature of the polymer, temperature of 20% weight loss of the polymer and the temperature at which the maximum decomposition rate occurred for the polymer, respectively. We can see the PVT polymer losses 20% weight of its structure at 323 ºC. On other hand, the PDT of nitrogen-rich salts of PVT polymer and their nanoparticles is in range of 235-245 ºC. It can be deduced from the data, the PVT polymer is more stable than its nitrogen-rich salts. Also, it is shown that the size of polymers is not important on stability of compound.

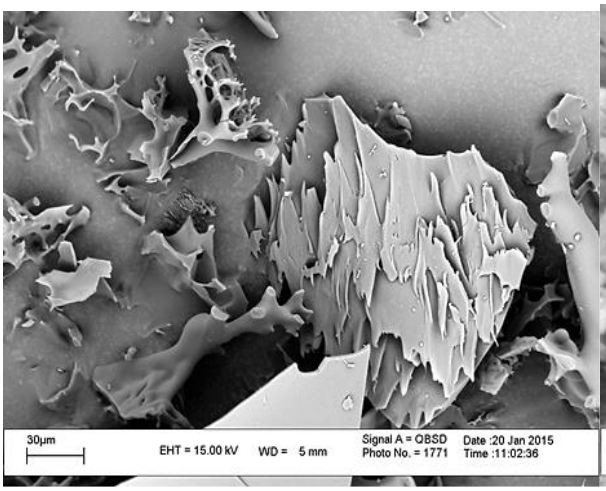

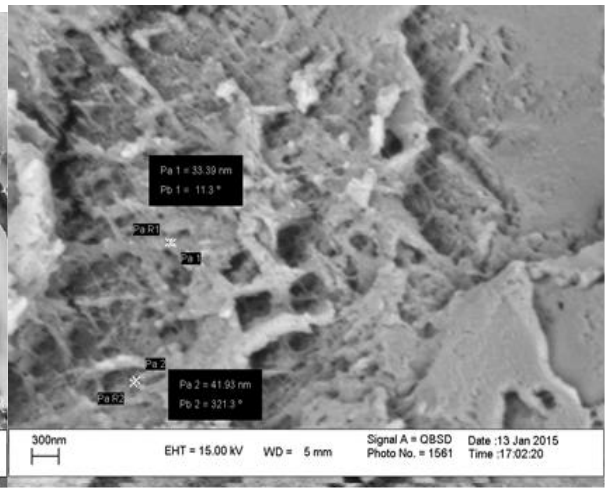

Figure 4. SEM image of APVT.Figure 5. SEM image of HPVT.

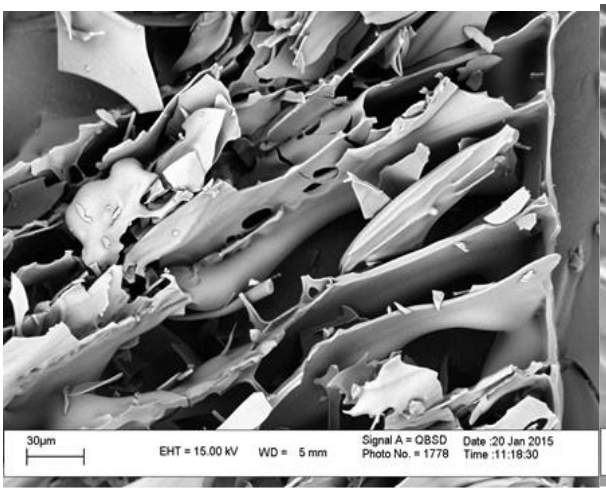

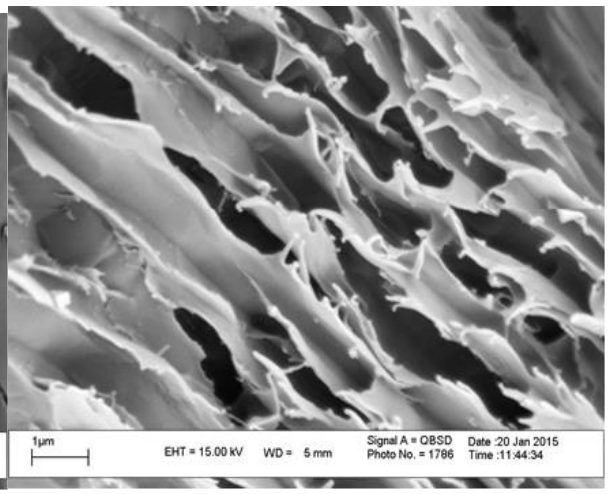

Figure 7. SEM image of AGPVT. Figure 6. SEM image of HAPVT.

Conclusions

The present work studies four nitrogen-rich polymer salts based on poly (5-vinilytetrazole) polymer. The compounds were synthesized in three steps. Firstly, the polyacrylonitrile (PAN) polymer was synthesized by free radical polymerization (FRP) approach. In second step, the tetrazole rings were prepared by reaction of nitrile groups and sodium azide. Then, the polynitrogen salts (APVT, HPVT, HAPVT and AGPVT) were prepared by reaction of PVT with ammonia, hydrazinium hydroxide, hydroxylamineand aminoguanidine bicarbonate, respectively. For make small the size of the mentioned four polymer salts, the polymers were frizzed and dried by the freeze-drying machine. The nitrogen-rich polymer salts indicate a detonation thermal degradation with a release of huge heat.

Acknowledgments

This work was supported by the AzarbaijanShahidMadani University, Tabriz, Iran.

Table 1. Thermal behavior of compounds.

Compound	IDT (°C)	PDT (°C)	PDT_{max} (°C)
PAN	147	720	912
PVT	141	323	870
APVT	142	233	690
HPVT	146	243	918
HAPVT	146	243	918
AGPVT	143	235	874
m-APVT*	146	242	919
n-HPVT*	147	243	919
m-HAPVT*	148	244	919
m-AGPVT*	146	245	920

* m and n present the size (micro and nano) of compounds.

References

[1]Agrawal, Jai Prakash. High energy materials: propellants, explosives and pyrotechnics. John Wiley & Sons, 2010.

[2] Akhavan, Jacqueline. The chemistry of explosives. Royal Society of Chemistry, 2011.

[3] Bratin, Karl, et al. "Determination of nitro aromatic, nitramine, and nitrate ester explosive compounds in explosive

mixtures and gunshot residue by liquid chromatography and reductive electrochemical detection." Analytica Chimica Acta 130.2 (1981): 295-311.

[4] Urbanski, Tadeusz, Marian/translated by Jurecki, and Sylvia/translated by Laverton. Chemistry and technology of explosives. Vol. 2. New York, NY: Pergamon Press, 1965.

[5] Girard-Lauriault, Pierre-Luc, et al. "Chemical Characterisation of Nitrogen-Rich Plasma-Polymer Films Deposited in Dielectric Barrier Discharges at Atmospheric Pressure." Plasma Processes and Polymers 5.7 (2008): 631-644.

[6] Gillan, Edward G. "Synthesis of nitrogen-rich carbon nitride networks from an energetic molecular azide precursor." Chemistry of materials 12.12 (2000): 3906-3912.

[7] Klapötke, Thomas M., and Davin G. Piercey. "1, 1′-Azobis (tetrazole): a highly energetic nitrogen-rich compound with a N10 chain." Inorganic chemistry 50.7 (2011): 2732-2734.

[8] Tappan, Bryce C., and Thomas B. Brill. "Thermal Decomposition of Energetic Materials 86. Cryogel Synthesis of Nanocrystalline CL-20 Coated with Cured Nitrocellulose." Propellants, Explosives, Pyrotechnics 28.5 (2003): 223-230.

[9] Ampleman, Guy, et al. "Synthesis of 14C-labelled hexahydro-1, 3, 5-trinitro-1, 3, 5-triazine (RDX), 2, 4, 6-trinitrotoluene (TNT), nitrocellulose (NC) and glycidylazide polymer (GAP) for use in assessing the biodegradation potential of these energetic compounds." Journal of Labelled Compounds and

Radiopharmaceuticals 36.6 (1995): 559-577.
[10] Arisawa, H., and T. B. Brill. "Thermal decomposition of energetic materials 71: Structure-decomposition and kinetic relationships in flash pyrolysis of glycidyl azide polymer (GAP)." Combustion and Flame 112.4 (1998): 533-544.
[11] Kawamoto, Aparecida M., et al. "Synthesis and Characterization of Glycidyl Azide-r-(3, 3-bis (azidomethyl) oxetane) Copolymers." Propellants, Explosives, Pyrotechnics33.5 (2008): 365-372.
[12] Desai, H. J., et al. "Synthesis of narrow molecular weight α, ω-hydroxy telechelic poly (glycidyl nitrate) and estimation of theoretical heat of explosion." Polymer 37.15 (1996): 3471-3476.
[13] McGrane, S. D., D. S. Moore, and D. J. Funk. "Shock induced reaction observed via ultrafast infrared absorption in poly (vinyl nitrate) films." The Journal of Physical Chemistry A108.43 (2004): 9342-9347.